

Contrasting effects of urbanization on vegetation between the Global South and Global North

Received: 11 August 2024

Accepted: 29 January 2025

Published online: 3 March 2025

 Check for updates

Jiuyi Chen  ¹, Bo Qiu  ^{1,2}✉, TC Chakraborty  ³, Xin Miao  ¹, Yipeng Cao ¹, Lingfeng Li ¹, Siwen Zhao ¹, Yueyang Ni ¹, Xiaohui Tian ¹, Yun Qian  ³ & Weidong Guo  ¹✉

Urban vegetation, the core component of green infrastructure and critical for sustainable cities, is profoundly affected by the process of urbanization. Urbanization not only leads to substantial vegetation loss (direct impact) but also fosters urban vegetation growth (indirect impact). However, the extent to which these direct and indirect impacts affect vegetation dynamics across cities worldwide and how urban greening will change in the future remain unclear. Using satellite-based greenness and impervious surface datasets, we show that positive indirect impacts mitigated 56.85% of the negative direct impacts across 4,718 cities worldwide from 2000 to 2019. Notably, the offsetting coefficient is much greater in Global North cities (79.13%) than in Global South cities (38.01%) partly due to their socioeconomic differences. This disparity in urban greening dynamics will continue in the future. Approximately 60% of Global North cities and 30% of Global South cities will become greener by 2040. Our results reveal the divergent trade-offs between vegetation loss and enhanced vegetation growth in cities of different socioeconomic levels and stages of urbanization. Such insights are crucial for a comprehensive understanding of urban greening dynamics and for devising strategies to attain sustainable development goals.

Human society has entered an urban age^{1,2}. With economic development and cultural shifts, many people have migrated from the countryside to cities, leading to unprecedented urbanization in recent decades^{2–4}. This process has led to tremendous ecological costs, including biodiversity loss^{5,6}, dramatic local environmental and climate changes^{7,8}, and profound impacts on vegetation growth^{9–11}. As an important regulator of the regional climate and environment, urban vegetation provides various ecological services for residents, including mitigating urban heat and the urban heat island (UHI) effect^{12–14}, affecting air quality^{15,16} and improving human health outcomes¹⁷. Driven by ongoing macro-climate changes and increasing urbanization, vegetation in cities and

peri-urban areas has undergone profound changes^{18,19}. However, the impacts of urbanization on vegetation dynamics remain inconsistent. Satellite-based vegetation greenness indices (a widely used measure to evaluate the coverage, growth and productivity of vegetation) reveal that urban vegetation has divergent trends across the globe^{18–21}. Since vegetation strongly controls urban environmental quality and livability, understanding the role of urbanization in regulating vegetation dynamics in cities and its expected effects in the future are vital for sustainable urban development.

The key to a comprehensive understanding of urbanization effects on vegetation dynamics is to separate the effects of urbanization on

¹School of Atmospheric Sciences, Nanjing University, Nanjing, China. ²Frontiers Science Center for Critical Earth Material Cycling, Nanjing University, Nanjing, China. ³Pacific Northwest National Laboratory, Richland, WA, USA. ✉e-mail: qjubo@nju.edu.cn; guowd@nju.edu.cn

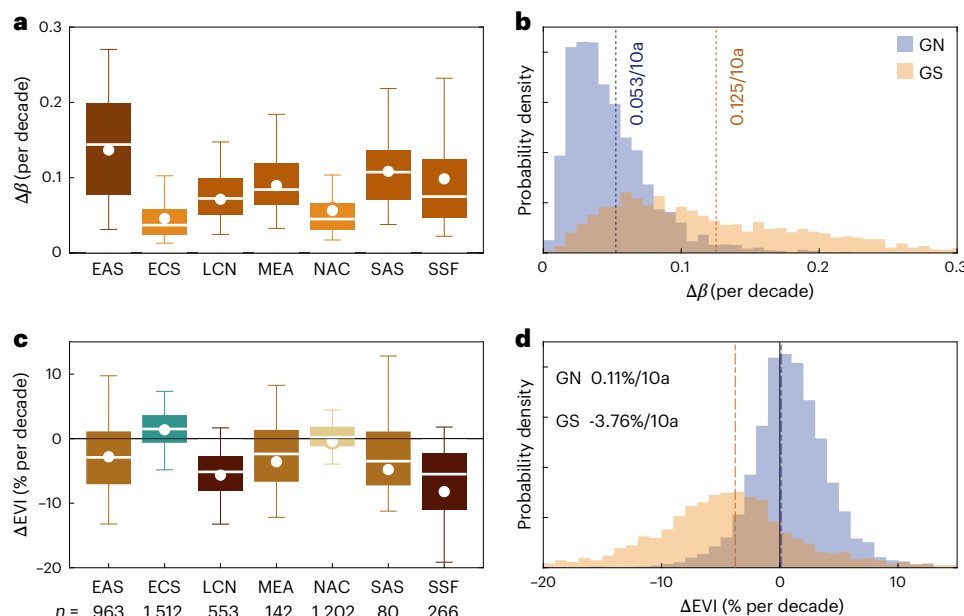


Fig. 1 | Increased urbanization and the changes in vegetation greenness in different parts of the world during 2000 to 2019. **a**, Changes in the fraction of impervious surface area ($\Delta\beta$) of cities in different regions of the world. EAS, East Asia and the Pacific, with city sample size of 963; ECS, Europe and Central Asia, 1,512 cities; LCN, Latin America and Caribbean, 553 cities; MEA, Middle East and North Africa, 142 cities; NAC, North America, 1,202 cities; SAS, South Asia, 80 cities; SSF, sub-Saharan Africa, 266 cities. These regions are defined by the

World Bank (<https://data.worldbank.org/country>). White lines represent the median $\Delta\beta$ for each region and white dots represent the average $\Delta\beta$ weighted by urban area for each region. Shaded boxes and vertical lines represent the ranges of 25–75% and 5–95%, respectively. **b**, Probability distributions of $\Delta\beta$ for Global North cities and Global South cities. Dotted lines are the average $\Delta\beta$ weighted by urban areas for the GN cities and GS cities. **c,d**, The same as in **a** and **b** but for relative changes in the EVI (ΔEVI).

vegetation cover and vegetation growth status^{22–24}. These two effects are also known as the direct and indirect effects of urbanization on vegetation^{22–24}. Specifically, direct impact refers to vegetation loss due to landcover transitions from natural vegetated surfaces to impervious surfaces such as roads, buildings and parking lots during urban expansion and densification. In contrast, indirect effects are due to vegetation growth enhancement from urban environmental changes (for example, longer photosynthetic season due to UHI effects, greater CO₂ fertilization effects) and result in urban vegetation composition differing from vegetation in the surrounding rural areas^{25–27}. In addition, human management measures such as choice of urban tree species, irrigation and fertilization can also affect urban vegetation growth^{27–29}. Several studies have separated direct and indirect urbanization effects by characterizing the relationship between urbanization intensity (fraction of impervious surface area) and the satellite-based vegetation index (VI) along urban–rural gradients^{22,24}. These studies suggested prevalent enhanced vegetation growth in urban environments. However, these studies, which are based on space-for-time frameworks, cannot provide the true temporal dynamics of urbanization-induced effects on vegetation^{18,23}. Furthermore, studies of differences in the direct and indirect impacts of urbanization on vegetation dynamics for cities at different stages of urbanization and different socioeconomic levels during historical periods and in the future are still lacking.

In this study, we provided a global analysis of urbanization effects on vegetation dynamics during 2000–2019 and the expected impacts in the future across 4,718 cities worldwide, using the satellite-based Enhanced Vegetation Index (EVI) and impervious surface area data^{30,31}. We quantified the direct and indirect impacts of urbanization on EVI variation for global cities and find that the offsetting coefficient (η) of indirect impact to direct impact is much higher in the Global North (GN) cities than in the Global South (GS) cities. We further investigated the contribution of their differences in climatic and socioeconomic characteristics to this disparity. Finally, we used machine learning models³², future urban fraction data³³ and socioeconomic data³⁴ to

project how this disparity in urban vegetation will change in the future. Our study focuses on the disparity in the direct and indirect impacts of urbanization on vegetation worldwide, particularly between GN and GS cities, and examines how socioeconomic characteristics and stages of urbanization contribute to these disparities. Addressing these questions is essential for understanding mechanisms of vegetation changes across global cities and offers important insights for making cities more resilient and sustainable amid increasing urbanization and global warming.

Increased urbanization and changes in urban vegetation

Rapid urbanization has led to a widespread rising fraction of impervious surfaces (β) in urban areas across cities worldwide (Extended Data Fig. 1). From 2000 to 2019, the average β of 4,718 cities worldwide has increased from 0.4661 to 0.6195 (Extended Data Fig. 2a). Among the seven regions across the world (Supplementary Fig. 1), East Asia and the Pacific have experienced the greatest increase in impervious surface area during the past two decades, followed by South Asia and sub-Saharan Africa (Fig. 1a and Extended Data Fig. 2b). Overall, cities that experienced rapid urban expansion ($\Delta\beta > 0.12$ per decade) during 2000–2019 are primarily located in emerging economies (for example, China, India and several countries in Africa) in the GS, whereas developed cities in the GN generally show a slight increase in β (Fig. 1b and Extended Data Fig. 1).

Rapid urban expansion was accompanied by substantial vegetation loss and exerted negative effects on vegetation greenness in urban areas, which is supported by the negative correlation between the urban expansion rate ($\Delta\beta$) and the ΔEVI ($r = -0.51$, $P < 0.01$). Most GS cities with marked impervious surface growth exhibit browning trends (Extended Data Fig. 1). However, the EVI in urban areas did not show an expected magnitude of decreasing trend. The average EVI across 4,718 cities worldwide decreased by only 0.0039 per decade (−1.55% per decade, Extended Data Fig. 2). Nearly half (45.2%) of the

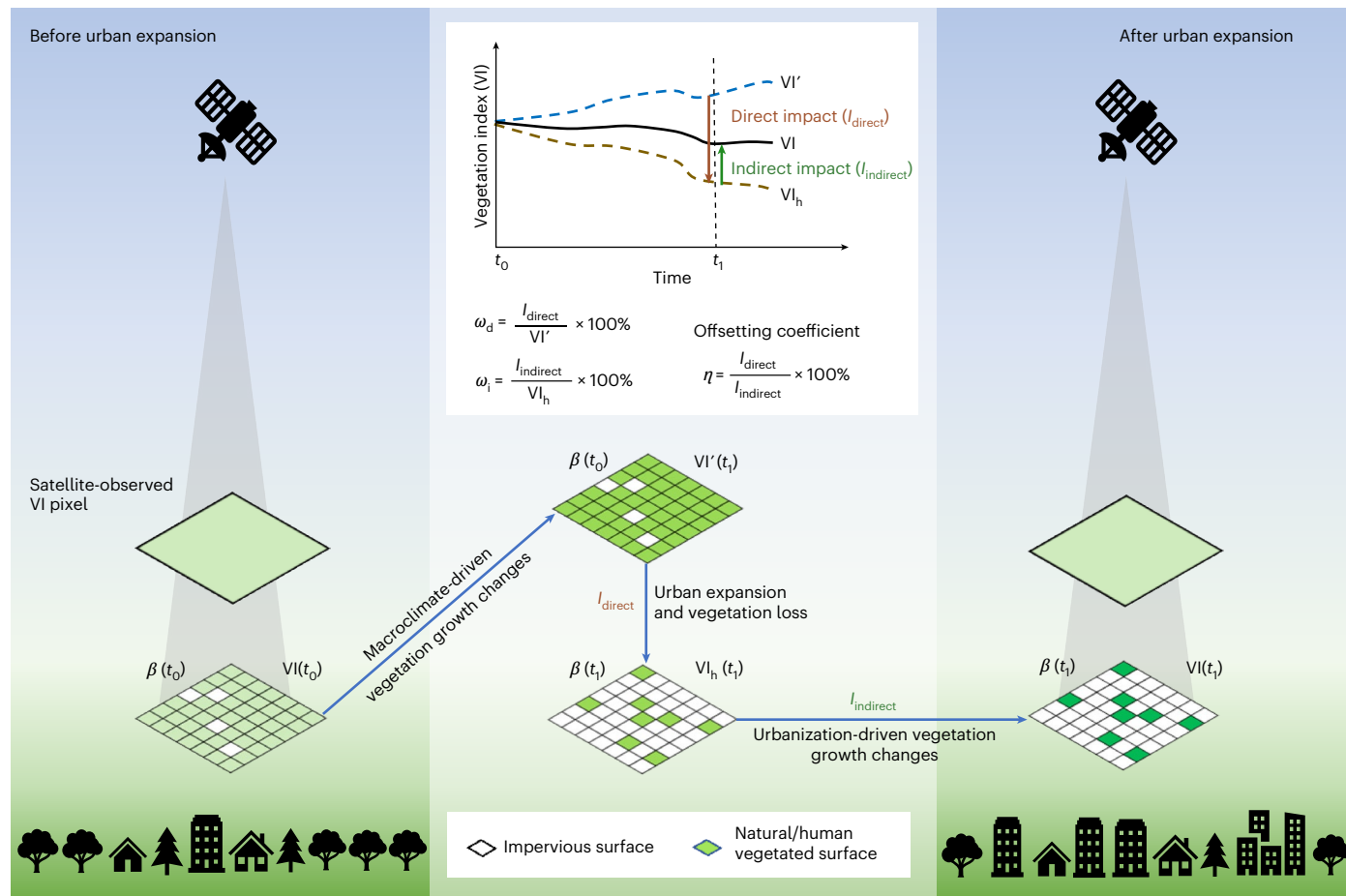


Fig. 2 | Schematic diagram of the effects of urbanization and macroclimate change on vegetation growth. The greenness-based vegetation index (VI) of an urban pixel can be decomposed into contributions from vegetated surfaces and non-vegetated surfaces (impervious surfaces). VI' (the blue dashed line) is the potential VI change without considering increased urbanization. Urbanization leads to vegetation cover loss through landcover transformation from vegetated surfaces to impervious surfaces, causing decreased VI. The brown dashed line represents the hypothetical VI (VI_h) that is affected only by macroclimate changes

and vegetation loss. The difference between VI_h and VI' is the direct impact of urbanization on the EVI (I_{direct}). ω_d is the percentage of VI decline caused by direct impact. The difference between the observed VI (black line) and VI_h is the indirect impact of urbanization (I_{indirect}), which indicates the response of vegetation growth to urbanization. ω_i is the percentage of vegetation growth variation caused by the indirect effects of urbanization. η is the offsetting coefficient of the indirect impacts to the direct impacts.

cities were greening from 2000 to 2019, most of which were in Europe, North America and Northeast Asia in the Global North (Fig. 1c,d). In particular, some cities in northern China (for example, Beijing) have experienced pronounced urban expansion and greening trends (Extended Data Fig. 1c and Supplementary Fig. 2).

Changes in urban EVI are the result of the joint effects of macroclimate changes and urbanization^{18,19}. To quantify the direct and indirect urbanization impacts on vegetation dynamics, we first separated the contributions of macroclimate changes to EVI variation (Fig. 2). The effects of macroclimate change were generally positive, leading to a global enhanced vegetation growth by +4.93% per decade (Extended Data Fig. 3). Without considering the effects of urbanization, macroclimate change resulted in a potential increase in the urban EVI of 0.010 per decade globally from 2000 to 2019 (Extended Data Fig. 3).

Direct and indirect impacts of urbanization on vegetation

We obtained the direct impacts of the changes in β (that is, loss of vegetation cover) on EVI (Fig. 2 and Supplementary Fig. 3). Consistent with the spatial distribution of $\Delta\beta$, GS cities generally experienced greater adverse direct impacts than GN cities did (Fig. 3a–c and Extended Data Fig. 4). Cities in China (for example, Chengdu) and West Africa experienced the most drastic urbanization and considerable direct impacts

on the EVI ($|\omega_d| > 20\%$ per decade), while cities in North America, Europe and Central Asia (for example, Chicago and Paris) experienced slight increases in impervious surface area ($\Delta\beta < 0.04$ per decade) and moderate direct impacts ($|\omega_d| < 10\%$ per decade) on the EVI from 2000 to 2019 (Fig. 3a and Supplementary Figs. 4–6). Globally, direct impacts resulted in an average decline in the EVI of 0.0324 per decade ($\omega_d = -11.93\%$ per decade) from 2000 to 2019 (Fig. 3c and Extended Data Fig. 4).

The indirect impacts of urbanization on the EVI were calculated from the differences between the observed VI and the hypothetical VI (VI_h), which considered both urbanization-induced vegetation loss and the response of vegetation growth to macroclimate change (Fig. 2). The indirect urbanization effects largely promoted vegetation growth in urban areas ($\omega_i = +9.31\%$ per decade), resulting in a global average increase in the EVI of 0.0184 per decade from 2000 to 2019 (Fig. 3d–f and Extended Data Fig. 4). In addition, the indirect impacts were positive in the vast majority (94.56%) of global cities, indicating prevalent vegetation growth enhancement in urban environments (Fig. 3c,d). Some cities in China presented the most pronounced positive indirect effects on vegetation growth ($\omega_i > 16\%$ per decade), and most cities in North America and Europe also typically presented, albeit smaller than the magnitudes seen for China, positive indirect effects ($\omega_i > 4\%$ per decade) (Fig. 3d,e). Among the seven regions, East Asia and the Pacific and sub-Saharan Africa had the greatest extent of vegetation growth

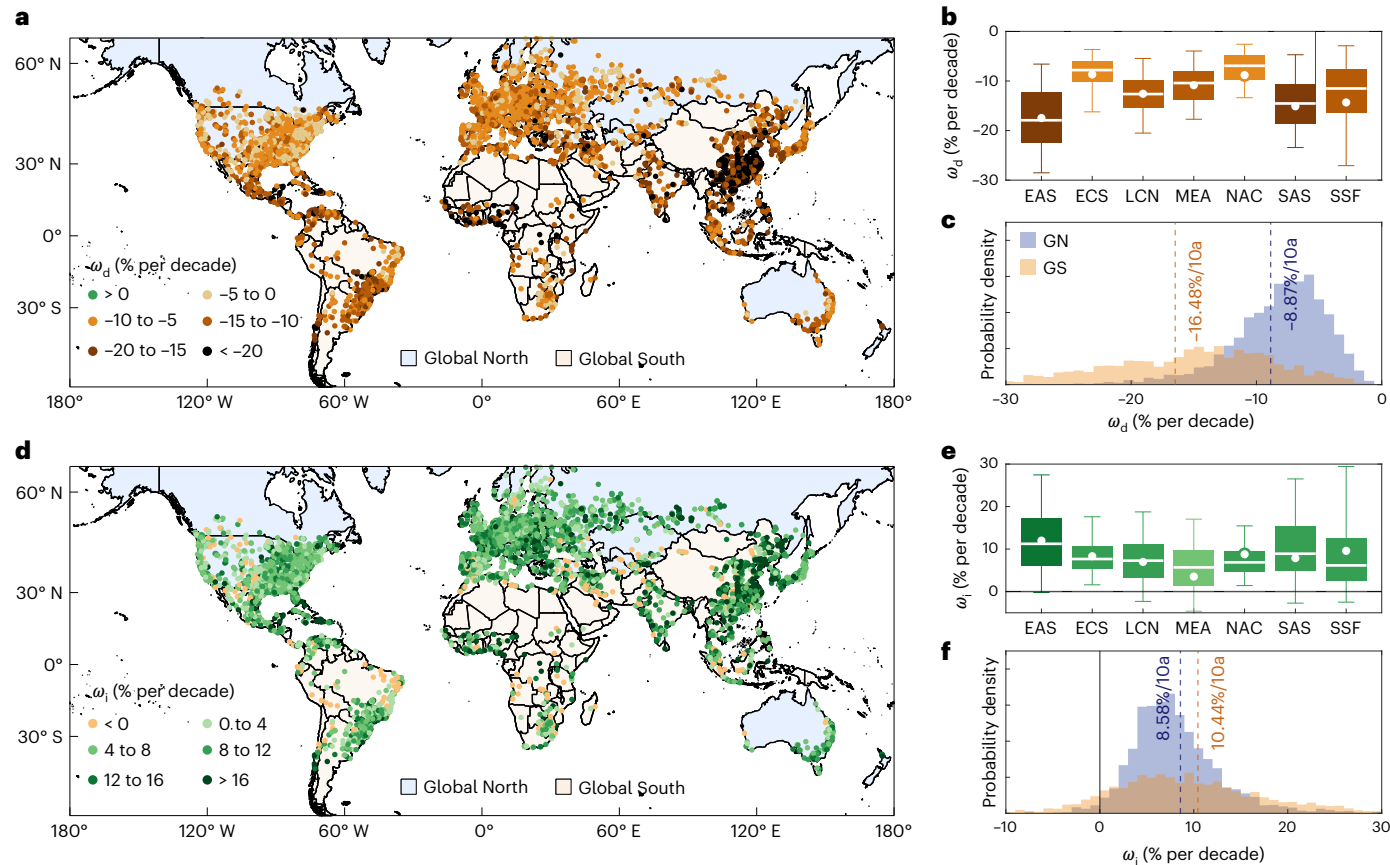


Fig. 3 | Direct and indirect effects of urbanization vegetation greenness from 2000 to 2019 across 4,718 cities worldwide. **a**, Magnitude of the EVI decline caused by the direct effects of urbanization (ω_d) during 2000 and 2019 across 4,718 cities. **b**, The ω_d of cities in different regions across the world. Abbreviations and number of cities for the different regions as in Fig. 1a. White lines represent the median $\Delta\beta$ for each region, and white dots represent the average $\Delta\beta$ weighted

by urban areas for each region. Shaded boxes and vertical lines represent the ranges of 25–75% and 5–95%, respectively. **c**, Probability distributions of ω_d for Global North and Global South cities. Dashed lines are the average $\Delta\beta$ weighted by urban areas for the GN and GS cities. **d–f**, The same as in **a–c** but for the magnitude of EVI variation caused by the indirect effects of urbanization (ω_i).

enhancement (Fig. 3e). Negative indirect impacts were observed in some cities (5.15%, for example, in Baghdad, Iraq) in the tropics or arid regions, most of which were in the Global South (Fig. 3d and Supplementary Fig. 7).

To explore how the indirect effects differ across global cities, we further investigated the influences of urbanization intensity, climatic and socioeconomic factors on the magnitude of vegetation growth enhancement driven by urbanization (ω_i) (Fig. 4a,b). We found a strong positive correlation between the rate of urban expansion ($\Delta\beta$) and ω_i ($r = 0.54, P < 0.01$), demonstrating increasing vegetation growth with more rapid urbanization (Fig. 4a). In addition, the urbanization intensity at the reference time (β_{2000}) is positively correlated with ω_i (partial correlation coefficient = 0.33, $P < 0.01$, Fig. 4b), indicating that vegetation growth was more promoted in cities that experienced earlier urbanization (higher β_{2000}). Controlling the urbanization intensity (β) and its trend ($\Delta\beta$), partial correlation analysis suggested a negative relationship between mean annual temperature (MAT) and ω_i (Fig. 4b). This indicates greater positive indirect impacts on vegetation growth in cold regions. Moreover, economic prosperity had a positive influence on urban vegetation growth (positive relationship between gross domestic product (GDP) per capita and ω_i , Fig. 4b). We also detected negative relationships between ω_i and the population density (partial $r = -0.17, P < 0.01$), the annual growth rate of population density (partial $r = -0.14, P < 0.01$) and economic growth rate (partial $r = -0.12, P < 0.01$) (Fig. 4b). Overall, the indirect effect of urbanization on vegetation growth is strongly affected by a city's socioeconomic characteristics and the stage of urbanization.

Contrast in offsetting coefficients between the GN and GS

The prevalent vegetation growth enhancement in urban environments can alleviate the adverse effects of vegetation losses due to urbanization. Here we used the offsetting coefficient (η , defined as the ratio of indirect impact to direct impact) to measure this compensation effect (Fig. 5). Globally, positive indirect impacts offset 56.85% of the negative direct impacts from 2000 to 2019, with an evident latitudinal pattern of η (Fig. 5a,b). Cities in the middle- and high-latitude regions in the Northern Hemisphere generally had greater offsetting coefficients (average $\eta = 72.61\%$ for cities north of 30°N) than other regions, and the tropical zones in the Southern Hemisphere present the lowest offsetting coefficient (average $\eta = 23.26\%$) (Fig. 5b). This disparity is associated with the background climate as cities in cold regions generally had greater indirect impacts on vegetation growth (Fig. 4b). In addition, the spatial heterogeneity of the offsetting coefficient is also closely associated with socioeconomic level, as suggested by the substantial and statistically significant positive correlation between η and the Human Development Index (HDI, a comprehensive measure of socioeconomic development) (Spearman's $r = 0.43, P < 0.001$, Fig. 5c).

Vegetation growth enhancement can offset a greater proportion of the negative impacts of vegetation loss in cities with high HDIs (Fig. 5c). On the one hand, cities with high HDIs generally had lower increase in impervious surface area ($\Delta\beta$) during 2000–2019, exerting less adverse direct impacts on vegetation (Extended Data Fig. 5a,b). On the other hand, higher HDIs are linked to higher GDP per capita ($r = 0.87, P < 0.01$) and lower population density ($r = -0.55, P < 0.01$). This leads

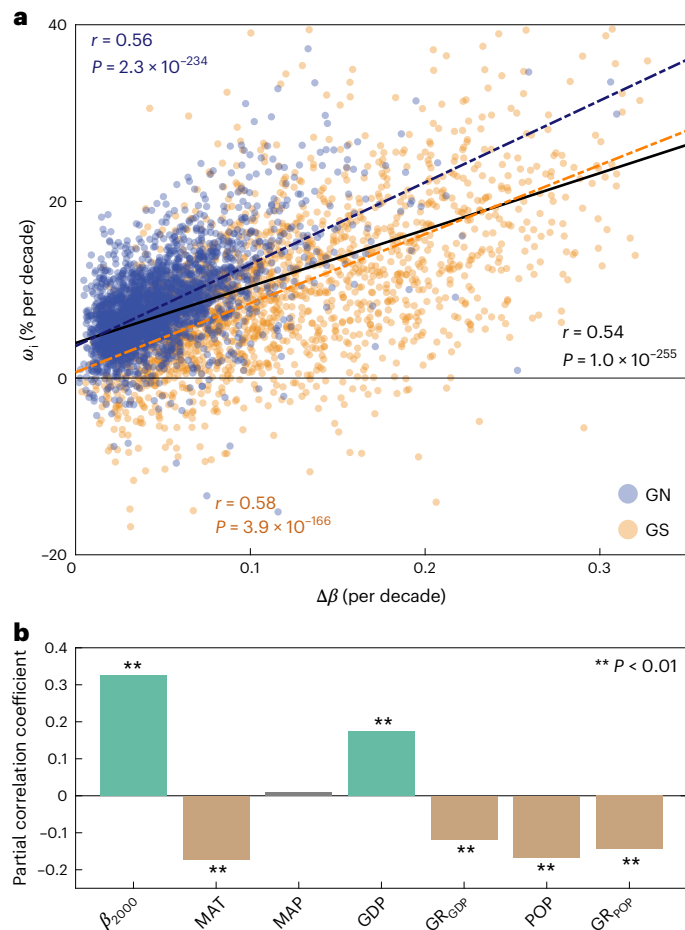


Fig. 4 | Vegetation growth enhancement driven by indirect effects of urbanization. **a**, Relationship between the indirect effects of urbanization on vegetation growth (ω_i) and the rate of urban expansion ($\Delta\beta$). Blue, orange and black lines denote the relationships between ω_i and $\Delta\beta$ for Global North cities ($P = 2.4 \times 10^{-234}, n = 2,888$), Global South cities ($P = 3.9 \times 10^{-166}, n = 1,830$) and for all cities ($P = 1.0 \times 10^{-255}, n = 4,718$), respectively. Statistical significance tests are based on two-sided Student's *t*-test. **b**, Partial correlation coefficients between ω_i and climatic and socioeconomic factors controlling urbanization intensity trend ($\Delta\beta$). β_{2000} , the urbanization intensity in 2000 ($P = 1.1 \times 10^{-117}$); MAT, mean annual temperature ($P = 7.9 \times 10^{-33}$); MAP, mean annual precipitation ($P = 0.5258$); GDP, purchasing power parity gross domestic product per capita in 2000 ($P = 5.4 \times 10^{-34}$); POP, population density in 2000 ($P = 1.2 \times 10^{-30}$); GR_{GDP}, compounded annual growth rate of GDP per capita since 2000 ($P = 3.4 \times 10^{-16}$); GR_{POP}, compounded annual growth rate of POP ($P = 3.9 \times 10^{-23}$). Statistical significance tests are based on two-sided Student's *t*-test. ** $P < 0.01$ ($n = 4,718$).

to greater vegetation growth enhancement in cities with high HDIs (Extended Data Fig. 5c). Notably, cities in the GN generally have higher HDIs than GS cities, with significant differences in η between GN and GS cities ($P < 0.01$, using the two-sided non-parametric Wilcoxon test) (Fig. 5d,e). The average η of GN cities is 79.13%, which is twice that of GS cities (38.01%). Moreover, 90.6% of cities with positive total effects of urbanization ($\eta > 100\%$) are in the GN, but 75.1% of cities with negative indirect impacts ($\eta < 0$) are in the GS (Fig. 5e). The differences in η between the GN and GS suggest the contrasting effects of urbanization on urban greening over the past two decades, which are closely associated with a city's socioeconomic level.

Projected urban EVI changes from 2020 to 2040

To project urban vegetation changes in the future, we used future urban cover fraction data, socioeconomic data and machine learning models to estimate the direct and indirect impacts of urbanization

on vegetation under three Shared Socioeconomic Pathways (SSP) by 2040 (Methods). Cities in East Asia and the Pacific are expected to have the most prominent vegetation degradation among the seven regions, with greatest EVI decline in southern China ($\Delta\text{EVI} < -20\%$) (Fig. 6). These regions are still in states of rapid urbanization and economic development, leading to great direct impacts on vegetation greenness (Extended Data Figs. 6–8). However, most cities in North America, Europe and Central Asia will become greener by 2040, with notably positive climatic and indirect impacts and moderate direct impacts (Fig. 6 and Extended Data Figs. 6–8).

Notably, the differences in the total effects of urbanization on vegetation between the GN and GS cities remain under the three SSP scenarios. The indirect urbanization impacts are expected to compensate for more direct impacts in the GN cities than in the GS cities (Extended Data Fig. 9). Thus, cities with greening trends are mostly in the GN, while most cities in the GS (~70%) will still be browning (Fig. 6c,f,i). Overall, global cities will be greener under the SSP1–Representative Concentration Pathways (RCP)2.6 scenario, with a higher ΔEVI (~0.93%) and proportion of greener cities (51.5%) than those under the SSP2–RCP4.5 (~−1.75%, 45.8%) and SSP5–RCP8.5 (~−2.29%, 45.2%) scenarios from 2020 to 2040.

Discussion

Rapid urbanization across the globe not only causes vegetation loss but also accelerates vegetation growth due to urban environmental changes, human management practices and urban greening policies^{22,24}. Previous studies have revealed divergent trends in urban vegetation dynamics, but the attribution of urbanization to vegetation dynamics often differs in direction and extent^{3,11,21}. In this work, we provide a global analysis of the historical impacts of urbanization on vegetation dynamics and projected vegetation changes in the future. By providing insight into the direct and indirect urbanization impacts on vegetation dynamics, our quantitative results at the global scale expand our understanding of vegetation responses to urbanization over space and time. In addition, our work separated the influences of macroclimate changes on vegetation growth, which largely reduced the uncertainty in estimating the impact of urbanization on vegetation dynamics. Our framework is also suitable for assessing urbanization-induced vegetation changes at the subcity scale, which can provide more details of vegetation responses to urbanization.

Our analysis demonstrates that the prevalent vegetation growth enhancement in urban areas offset over half of the negative direct effects of urbanization across global cities during 2000–2019. In particular, our results demonstrate the contrast in the total impacts of urbanization on vegetation between cities in the GS and GN, and the contrast will persist under different scenarios in the future. This contrast is primarily associated with differences in their stage of urbanization. The process of industrialization in most Global South countries (for example, China, India and many African countries) began after the mid-twentieth century^{3,4}. The mass migration of people to cities occurred at the end of the twentieth century and the beginning of twenty-first century¹³. This caused remarkable urban expansion³⁵ and considerable adverse direct impacts on vegetation (Fig. 3) in East Asia, South Asia and Africa. Global North cities, however, have expanded mildly since 2000, with slight negative direct impacts but notable positive indirect impacts on vegetation growth (Fig. 3). The notable positive indirect effects might be due to more well-established green spaces that have more structurally developed vegetation (for example, trees and shrubs) in these mature cities²⁰. Besides, we also notice another type of city with a trajectory of both slight direct and indirect impacts of urbanization on vegetation. These cities are mainly in the Middle East and South America, which have been highly urbanized in the late twentieth century. However, the population growth in cities surpasses the economic level and urban infrastructure capacity in these regions, which are considered to be 'over-urbanized'^{4,36}.

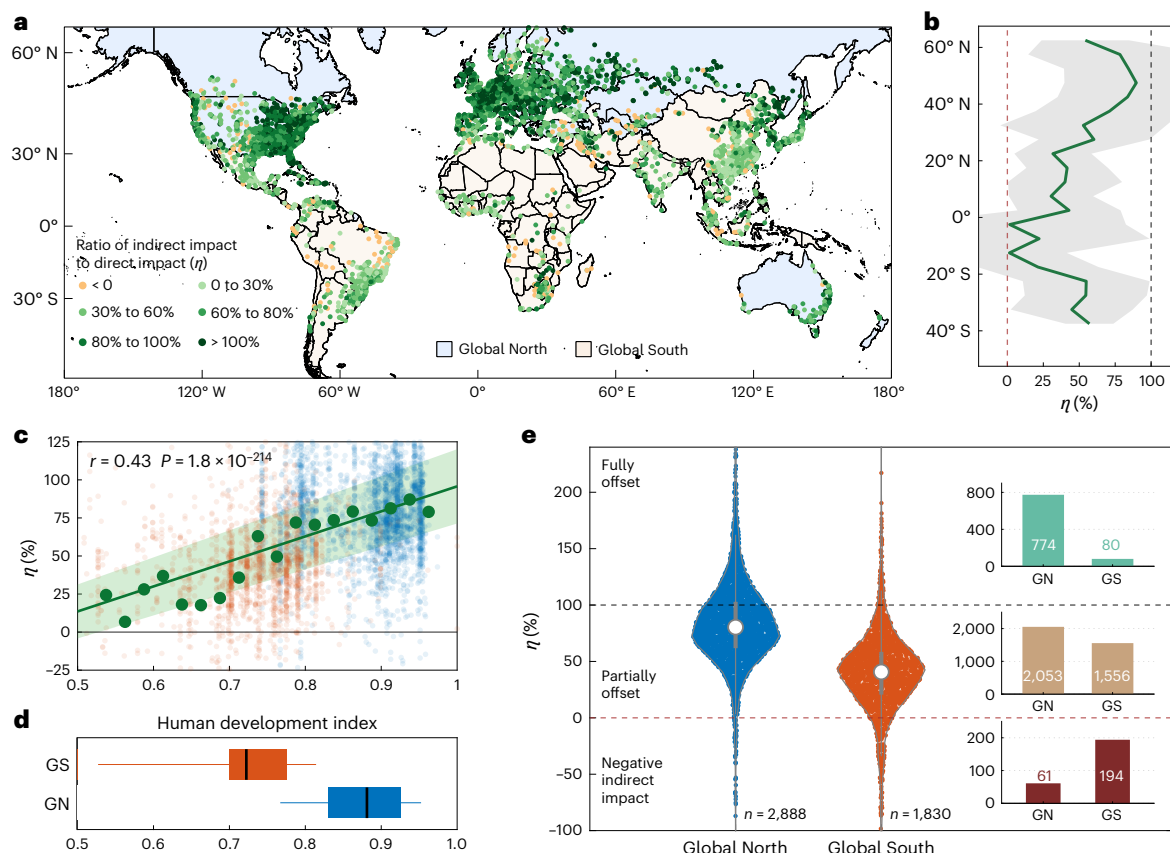


Fig. 5 | Differences in the offsetting coefficients of the indirect impacts to direct impacts across 4,718 cities worldwide. **a**, Offsetting coefficients (η) of the indirect impacts to the direct impacts across 4,718 cities worldwide. **b**, Latitudinal pattern of η . Green line and shaded areas represent the means and standard deviations of the cities in each latitudinal bin, respectively. **c**, Relationship between η and a city's socioeconomic development level defined by the human development index (HDI). Small red and blue dots denote GN and GS cities, respectively. The η for cities at different development levels are averaged

by each 0.025 HDI bin, and each green dot represents a bin. Solid lines and shaded areas indicate significant trends and 95% confidence intervals. Significance was determined using two-sided Student's *t*-test ($n = 4,718$). **d**, Distributions of HDIs of cities in the GS and GN. Black lines represent the average value of each variable for GS ($n = 2,888$) and GN ($n = 1,830$) cities. Shaded boxes and horizontal lines represent the ranges of 25–75% and 5–95%, respectively. **e**, Distribution of η for GN ($n = 2,888$) and GS ($n = 1,830$) cities. Hollow circles represent the average η for GN and GS cities. Bar charts show the numbers of cities in different η ranges.

This might exert greater ecological pressure on the environment with less green infrastructures in urban areas^{4,20}. The differences in the direct and indirect impacts of urbanization across global cities indicate the divergent trade-offs between urbanization and ecological conservation among cities at different stages of development.

Our results reveal that the differences in urban vegetation dynamics between GN and GS cities are also closely related to their socioeconomic characteristics, which affect the indirect effects of urbanization on vegetation growth. The developed cities in the GN generally have higher economic levels than do the GS cities (Extended Data Fig. 10). The positive correlation between GDP per capita and the indirect effects (ω_i) indicates the role of artificial management measures in urban greening dynamics as wealthier cities or communities usually invest more in urban green infrastructure to improve environmental quality and greenspace supply for residents (Fig. 4b and Supplementary Fig. 8)^{19,37,38}. In addition, we detected negative influences of dense population and high economic growth rate on urban vegetation growth (Fig. 4b). A dense population and rapid economic development would exert greater pressure on the urban environment, leading to a negative influence on vegetation growth^{19,20}. Compared with the developed cities in the GN, GS cities have much higher population densities (about three times that of GN cities) and population growth rate (more than twice that of GN cities) (Extended Data Fig. 10). In addition, urbanization in the GS was accompanied by more rapid economic development (Extended Data Fig. 10). Overall, GN cities commonly experienced

greater positive indirect urbanization effects on vegetation growth than the GS cities and have greater offsetting coefficient of indirect effect to direct effect (Fig. 5e). Recent studies have revealed the contrast in infrastructure^{37–39}, human exposure to green spaces⁴⁰ and the cooling benefits of greenspace¹⁴ among cities in the GN and GS. The divergent greening trends of the GN and GS cities would lead to greater inequality in human exposure to green spaces. Because of the important role of urban vegetation in reducing human exposure to high temperatures and heat stress^{12–14}, providing health benefits¹⁷ and augmenting residents' living comfort, the United Nations underscores the necessity of 'providing universal access to greenspace for urban residents' as part of the 11th Sustainable Development Goals⁴¹. Rational city planning that considers both urban expansion and urban renewal is urgently needed to balance the trade-off between urban development and its ecological and environmental consequences in Global South cities. Increasing regional or international economic aid would help to increase investment in urban greening in GS cities, which is beneficial to achieve equitable urban greening ecosystem services across the world.

Some levels of uncertainty and limitations should be acknowledged. First, uncertainties in the impervious surface and EVI datasets should be noted. Due to differences in data sources, spatial resolutions and algorithms used for inversion, there are some discrepancies in estimates of impervious surface area from datasets across scales^{31,42}. Here we used the GISA 2.0 dataset with a high resolution of 30 m, which considers the consistency of some existing products and is more accurate

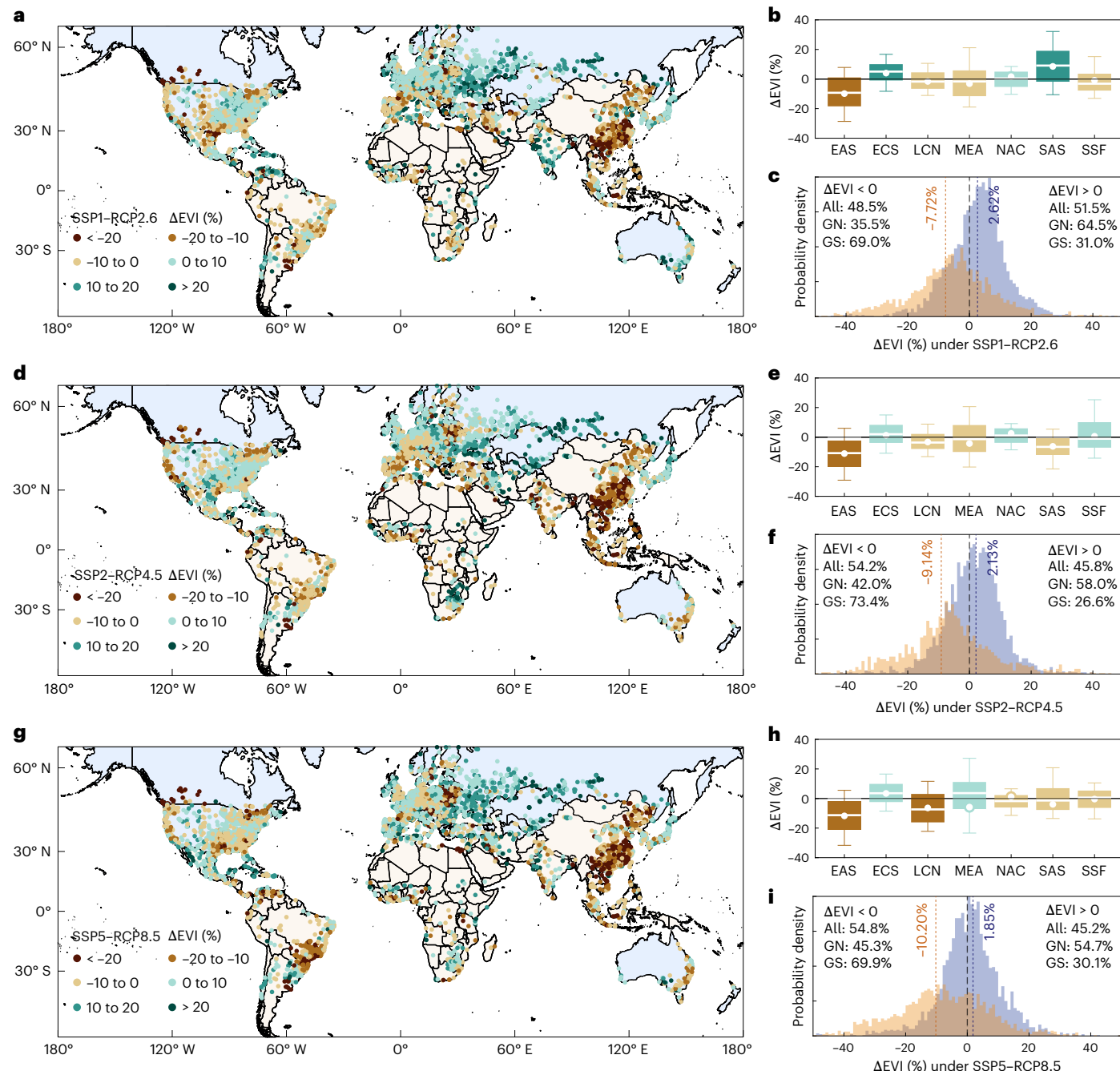


Fig. 6 | The projected vegetation changes of global cities under different Shared Socioeconomic Pathways from 2020 to 2040. **a**, Estimated ΔEVI by 2040 across global cities under SSP1-RCP2.6. **b**, ΔEVI of cities in different regions across the world. Abbreviations and number of cities for the different regions as in Fig. 1a. White dots represent the average $\Delta\beta$ weighted by urban areas for each region. Shaded boxes and vertical lines represent the ranges of 25–75% and

10–90%, respectively. **c**, Probability distribution of ΔEVI for the cities in the GN and GS. Dotted lines are the average ΔEVI weighted by urban areas for GN and GS cities. The numbers are the proportions of cities with positive or negative ΔEVI values. **d–f**, The same as in **a–c** but for ΔEVI under the SSP2-RCP4.5 scenario. **g–i**, The same as in **a–c** but for ΔEVI under the SSP5-RCP8.5 scenario.

and stable³¹. Even so, unrecognized green spaces or buildings due to data resolution might result in misestimation of the direct and indirect impacts^{20,42}. For example, many residential gardens and street trees are smaller than the 30 m landcover pixel, potentially leading to an underestimation of vegetation cover^{20,42,43}. Advances in remote sensing technology, such as more accurate land cover with finer resolution and detailed characterization of the functional type and structure of urban vegetation, would be helpful for improving the understanding of urban greening dynamics and associated drivers in future studies. Second, the responses of vegetation growth to urbanization may

vary at temporal and spatial scales across different parts of a city. For instance, previous studies have revealed the disparities in vegetation dynamics between urban cores and urban fringes (greening in the centre while browning in expansion areas)^{18,43} and between rich zones and slum areas (for example, green gentrification)⁴⁴. In this study, we focus on the average impacts at the city scale, and the prediction of future urban vegetation change is limited to existing urban areas. Future studies can apply our framework at the subcity scale and in specific regions to access details of urbanization-induced vegetation changes. Third, indirect urbanization impacts are the combined result

of various interacting biogeochemical mechanisms (for example, extended growing seasons, greater CO₂ fertilization effects, elevated nitrogen deposition) and anthropogenic factors (for example, urban planning, the species composition of urban vegetation and investment in green infrastructure)^{18,22,26}. Although the significant positive correlation between the rate of urban expansion and ω_1 demonstrates the benefits of urban environmental changes on vegetation growth (Fig. 4a), it is still challenging to differentiate the contribution of each potential mechanism. Future studies on the attribution of urban vegetation changes are crucial for understanding the mechanisms of vegetation responses to future urbanization and climate change^{5,22,25}.

Methods

Urban boundary and impervious surface area

The multitemporal global urban boundary (GUB) dataset⁴⁵ was used to extract the urban areas in our study. The GUB dataset is based on the spatial distribution of artificial impervious areas from Landsat data and can capture the complicated shapes of urban extent well. We selected cities with areas larger than 10 km² in 2018, which included both metropolitan cities and many small cities that house millions of urban residents. The study area for each city was the urban area in 2018.

The global impervious surface area dataset (GISA 2.0) was used to quantify the fraction of impervious surfaces (β)³¹. This dataset has long-term records from 1985 to 2019 with a spatial resolution of 30 m. Compared with existing global impervious surface datasets, the GISA 2.0 dataset considers the consistency of existing products and is more accurate and stable³¹. We aggregated the GISA 2.0 dataset to 500 m resolution and calculated the fraction of impervious surfaces of each 500 m pixel. The values of β ranged from 0 (fully vegetated surface) to 1 (fully built-up surface). We calculated the β for each city per year and their trends from 2000 to 2019.

The projected urbanization intensity in 2040 was obtained from a global dataset of urban fractions with a 1-km resolution. This dataset provides urban fraction data under eight SSP–RCP scenarios from 2020 to 2100 (5-year interval), which can explicitly capture the gradual variations in impervious surface area within pixels³³. We calculated the changes in the urbanization intensity ($\Delta\beta$) of each city between 2020 and 2040 under three SSP–RCP scenarios (SSP1–RCP2.6, SSP2–RCP4.5 and SSP5–RCP8.5) to estimate the projected direct impacts of urbanization on vegetation greenness in urban areas.

Satellite-based vegetation index

The EVI with a 500 m spatial resolution from the MODIS data products (MOD13A1 v.6.1) was used as an indicator of vegetation growth state in this study³⁰. EVI minimized canopy background variations and removed residual atmosphere contamination caused by smoke and subpixel thin cloud clouds using the blue band. We filtered the pixels with low confidence using the quality assessment layer and then integrated the 16-day EVI to yearly data by calculating the annual mean EVI from March of each year to February of the following year since the MOD13A1 product is only available since 18 February 2000. We used the annual average EVI for each 500-m pixel and calculated the annual mean EVI for each city to represent the average state of urban vegetation from 2000 to 2019. We also calculated the annual mean leaf area index (LAI) for each city using the MODIS LAI products (MOD15A2H)⁴⁶. We addressed the relationship between EVI and LAI to estimate the future climatic impact on the urban EVI. The R² of the quadratic regression between the LAI and EVI (LAI = $(a \times \text{EVI} + b)^2$) is 0.591 (Supplementary Fig. 9).

Climatic and socioeconomic factors

The climate data were obtained from the TerraClimate dataset. TerraClimate is a dataset of the monthly climate and climatic water balance for global terrestrial surfaces since 1958⁴⁷. This dataset provides time-varying climate data with high spatial resolution for ecological and hydrological studies. All the data have a monthly temporal

resolution and a ~4-km spatial resolution. We extracted the 2-m air temperature, precipitation and the potential evapotranspiration (PET) to calculate the mean annual temperature (MAT), mean annual precipitation (MAP) and aridity index (AI, defined as the ratio of MAP to PET) for each city from 2000 to 2020.

Global gridded datasets for the HDI and GDP produced by ref. 48 were used in this study. This dataset provides the global 5-arc-min-resolution purchasing power parity GDP per capita, total GDP and HDI for the period 1990–2015. The HDI, a quantitative index that measures key dimensions of human development, was used to describe socioeconomic development of global cities. We extracted the average HDI and GDP per capita from 2000 and 2015 for each city. We also calculated the compound annual growth rate of GDP per capita (GR_{GDP}) for each city to measure the rate of economic development. The population density in urban areas and its compound annual growth rate (GR_{POP}) were derived from gridded global population density dataset with a 1-km spatial resolution produced by the WorldPop group⁴⁹.

The projected population density and GDP data were derived from gridded datasets for the population and economy under Shared Socioeconomic Pathways³⁴. Based on the Population–Development–Environment (PDE) model and the Cobb–Douglas production model with localized population and economic parameters, the dataset provides gridded SSP population and economic data from 2020–2100 under five Shared Socioeconomic Pathways (SSPs)⁵⁰. We calculated the rate of population density (GR_{POP}) and average GDP per capita (GR_{GDP}) from 2020 to 2040 for each city to predict the indirect effects of urbanization.

Digital elevation and landcover

The digital elevation data used for rural pixel screening were derived from the Global 30-m Digital Elevation Model (GLO-30) from Copernicus⁵¹. The digital elevation data were resampled to a 500-m resolution. The 500-m landcover data were acquired from the MCD12Q1 v.6.1 product, which is derived using supervised classification of MODIS Terra and Aqua reflectance data⁵². We used the landcover types defined by the International Geosphere–Biosphere Programme (IGBP) classification schemes. When calculating the vegetation growth variation in rural areas, we excluded the pixels identified as non-vegetational cover or human managed types (that is, croplands, urban and built-up areas, croplands/natural vegetation mosaics, snow and ice, and barren) and the pixels that experienced landcover changes from 2001 to 2018. Only the natural vegetation pixels without major landcover type changes were used in the analysis.

Separating the direct and indirect impacts

Schematic diagrams of this framework are shown in Fig. 2 and Supplementary Fig. 2. The VI of a pixel is determined by the vegetation coverage and the greenness of the vegetated surface. Following the conceptual framework proposed by ref. 22, we assumed that the VI of an urban pixel decreases linearly with increasing urban intensity (β , represented by the proportion of impervious surfaces within a VI pixel):

$$\text{VI} = \text{VI}_v \times (1 - \beta) + \text{VI}_{nv} \times \beta \quad (1)$$

where VI_v is the value of VI if the pixel was completely filled by vegetated surfaces with the current growth condition ($\beta = 0$), and VI_{nv} is the minimum VI at the pixels completely filled by built-up surfaces ($\beta = 1$). The VI here can be either the EVI or other vegetation-related variables, such as gross primary productivity (GPP) or net primary productivity (NPP). For the EVI, the value of VI_{nv} was set as 0.05 according to previous studies, by assuming that an EVI lower than 0.05 generally has no vegetation activity^{22,24}. At the reference time t_0 , VI_v can be obtained by:

$$\text{VI}_v(t_0) = \frac{\text{VI}(t_0) - \text{VI}_{nv} \times \beta(t_0)}{1 - \beta(t_0)} \quad (2)$$

where $\beta(t_0)$ is the fraction of impervious surface of the pixel at the reference time t_0 .

Without considering the effects of increasing urbanization, the temporal variation in VI ($VI'(t_1)$) is affected only by background biogeochemical drivers:

$$VI'(t_1) = \gamma \times VI_v(t_0) \times (1 - \beta(t_0)) + VI_{nv} \times \beta(t_0) \quad (3)$$

where γ is the relative magnitude of VI variation driven only by macroclimate change. However, urbanization leads to landcover transformation from vegetated surfaces to impervious surfaces, manifested as increased β and decreased vegetation coverage. The hypothetical VI at t_1 ($VI_h(t_1)$) that considers both urbanization-induced vegetation loss and vegetation growth changes driven by macroclimate change can be obtained as follows:

$$VI_h(t_1) = \gamma \times VI_v(t_0) \times (1 - \beta(t_1)) + VI_{nv} \times \beta(t_1) \quad (4)$$

where $\beta(t_1)$ is the fraction of the impervious surface of the pixel at time t_1 . The direct impact of urbanization on VI was then calculated by the difference between $VI_h(t_1)$ and $VI_v(t_1)$:

$$I_{\text{direct}} = -(\beta(t_1) - \beta(t_0)) \times (\gamma \times VI_v(t_0) - VI_{nv}) \quad (5)$$

The relative magnitude of the direct effect of urbanization on VI is as follows:

$$\omega_d = \frac{|I_{\text{direct}}|}{VI'(t_1)} \times 100\% \quad (6)$$

However, the actual VI at t_1 is usually different from that at $VI_h(t_1)$ because of changes in urbanization-driven vegetation growth. The difference between the observed VI and the hypothetical VI was then considered the indirect impact of urbanization on the VI:

$$I_{\text{indirect}} = VI(t_1) - VI_h(t_1) \quad (7)$$

The magnitude of vegetation growth variation driven by indirect urbanization effects (ω_i) is the quotient of the indirect impact over $VI_h(t_1)$:

$$\omega_i = \frac{|I_{\text{indirect}}|}{VI_h(t_1)} \times 100\% \quad (8)$$

The offsetting coefficients of indirect impacts to direct impacts are defined as follows:

$$\eta = \frac{|I_{\text{indirect}}|}{|I_{\text{direct}}|} \times 100\% \quad (9)$$

To eliminate the effects of interannual fluctuations and disturbances from extreme events, we used the temporal trends of ω_d and ω_i from 2000 to 2019 in the main text.

Separating the effects of macroclimate change

Direct and indirect impacts can be obtained if the effects of macroclimate change on vegetation growth (γ) are known. To acquire γ in urban areas, we propose an adjacent substitution method on the basis of two assumptions: (1) the magnitude of the effects of large-scale climate change on vegetation growth in urban areas is roughly the same as that in the rural area around a city (spatial homogeneity of γ) and (2) the exurban rural areas are not affected by the indirect effects of urbanization ($\omega_{\text{rural}} \approx 0$). Then, we use the median γ of the pixels that satisfy the two assumptions as a substitute for that in urban areas.

A flow chart of the process of city screening and adjacent substitution is shown in Supplementary Fig. 10. We used the urban boundary

dataset to extract the urban areas and the rural areas around the cities⁴⁵. Global cities (9,227) with areas larger than 10 km² in 2018 were first selected for analysis. To obtain the surrounding rural areas, we created two buffers outwards for each city. The buffer distances of the inner and outer buffers were determined by the size of the urban area to avoid the drawback of adopting a fixed threshold for cities of different sizes²⁴.

$$D_{\text{inner}} = (\sqrt{2} - 1) \times \sqrt{\frac{S}{\pi}} \quad (10)$$

$$D_{\text{outer}} = (\sqrt{10} - 1) \times \sqrt{\frac{S}{\pi}} \quad (11)$$

where S is the size of a city in 2018. The inner buffer is the same as the size of the urban area under the assumption of a circular shape of a city. The outer area without the inner buffer area is approximately eight times the size of the city. We suppose that only the vegetation in urban areas and inner buffers would be affected by the indirect effects of urbanization. The rural area between the inner buffer line and the outer buffer line was used to calculate the effects (γ) of background drivers for each city. Areas within inner buffer lines of other cities were also excluded to meet the requirements of Assumption 2 if a city's outer buffers contained them.

For the selected nearby rural areas, the pixels with elevations greater than 100 m from the mean elevation of the urban area were filtered to satisfy Assumption 1 of the spatial uniformity of climate change effects. In addition, only the pixels that were identified as natural vegetation in the MODIS landcover map (MCD12Q1) and that had not experienced landcover change were used to calculate γ in rural areas, considering that croplands are profoundly affected by anthropic factors. We then calculated the median γ for the remaining pixels in rural areas as the replacement value of γ in urban areas to avoid the influence of extreme values. In addition, cities without valid GDP, HDI or population density data were also excluded. After city screening, 4,718 cities were selected in this study. We divided the cities into GS cities and GN cities and further grouped them into seven subregions according to the World Bank (Supplementary Fig. 1).

Statistical analysis

Statistical analyses and plotting were conducted in MATLAB R2021b. To characterize the correlation between different variables, we used Pearson's correlation coefficient. Statistically significant tests are set at the 0.01 probability level based on two-sided *t*-tests.

Estimating future urban vegetation changes

Considering that urbanization is expected to continue in the future, we estimated the projected EVI changes from 2020 to 2040 for global cities under three SSP–RCP scenarios. According to the previous framework, the projected EVI at some time in the future can be obtained using the following equation:

$$VI(t_2) = \gamma' \times VI_v(t_1) \times (1 - \beta(t_2)) \times (1 + \omega') + VI_{nv} \times \beta(t_2) \quad (12)$$

$VI_v(t_1)$ is the VI of per unit vegetated area of a pixel in 2020. $\beta(t_1)$ and $\beta(t_2)$ are the urbanization intensities in 2020 and 2040, respectively. The urbanization intensity in 2040 ($\beta(t_2)$) can be obtained from the aforementioned future urban fraction dataset. γ' and ω' represent the effects of macroclimate change and the indirect effect of urbanization on vegetation growth, respectively.

The effects of macroclimate change on vegetation (γ') were derived from the projected vegetation changes of nine models from the six Coupled Model Intercomparison Project (CMIP6) (Supplementary Table 1). Six of the earth system models (BCC-CSM2-MR⁵³, CanESM5 (ref. 54), EC-Earth3-Veg⁵⁵, EC-Earth3-Veg-LR⁵⁵, GFDL-ESM4 (ref. 56) and IPSL-CM6A-LR⁵⁷) use dynamic vegetation models. The INM-CM4-8

and INM-CM5-0 models have a carbon cycle module with a prescribed potential vegetation distribution, and the root-zone soil moisture was used to determine the actual vegetation⁵⁸. The carbon cycle module of the MPI-ESM1-2-LR model was also simulated by land use and vegetation changes⁵⁹. All nine models provide vegetation change data under climate change.

We first used the LAI of each CMIP6 earth system model to calculate the projected EVI changes under different SSPs, using the quadratic relationship between the LAI and EVI from historical datasets. We then calculated the multimodal ensemble average EVI of the nine earth system models. Considering that the resolution of these models (-1°) is much larger than the city scale, we assumed that the influence of urbanization is slight and that the vegetation changes are driven primarily by background factors. The effect of macroclimate changes on vegetation growth (γ') is approximately the EVI variation of the grid where a city is located:

$$\gamma' = \frac{\text{EVI}(t_2)}{\text{EVI}(t_1)} \quad (13)$$

For the indirect effects of urbanization (ω'), we first used the boosted regression tree (BRT) model to address the relationships between the indirect effects (ω) and climatic and socioeconomic factors, including the mean annual temperature (MAT), aridity index (AI), the effect of macroclimate change on vegetation growth (γ), urbanization intensity at the reference time ($\beta(t_0)$), rate of urban expansion ($\Delta\beta$), GDP per capita (GDP), rate of economic development (GR_{GDP}), population density (POP) and population growth rate (GR_{POP}).

$$\omega \sim \text{MAT} + \text{AI} + \beta(t_0) + \Delta\beta + \text{GDP} + \text{GR}_{\text{GDP}} + \text{POP} + \text{GR}_{\text{POP}} \quad (14)$$

The BRT model is a tree-based machine learning model that can address complex nonlinear relationships between dependent variables and predictors³⁵. The BRT model (training correlation = 0.9047, cross-validation (CV) correlation = 0.7485) suggests that the nine explanatory variables can explain 78.87% of the variance of the indirect effects. The parameters of the BRT model (that is, tree complexity, learning rate and bag fraction) were optimized by improving the model's CV correlation with different combinations of parameters^{32,60}. The tree complexity, learning rate and bag fraction were then set as 10, 0.005 and 0.6, respectively (Supplementary Table 2). The number of trees in the BRT model was determined through a CV procedure. We then used the projected variables to predict the indirect impact and obtain ω' . The direct, indirect and climatic impacts on urban EVI were obtained as follows:

$$I'_{\text{climatic}} = (\text{VI}(t_1) - \text{VI}_{\text{nv}} \times \beta(t_2)) \times (\gamma' - 1) \quad (15)$$

$$I'_{\text{direct}} = -(\beta(t_2) - \beta(t_1)) \times (\text{VI}_v(t_1) - \text{VI}_{\text{nv}}) \times \gamma' \quad (16)$$

$$I'_{\text{indirect}} = \gamma' \times \text{VI}_v(t_1) \times (1 - \beta(t_2)) \times \omega' \quad (17)$$

Reporting summary

Further information on research design is available in the Nature Portfolio Reporting Summary linked to this article.

Data availability

The datasets in this study are publicly available as follows or can be obtained from Google Earth Engine. MODIS vegetation greenness data (MOD13A1) and landcover data (MCD13Q1) are available at <https://ladsweb.modaps.eosdis.nasa.gov>. GTOPO30 digital elevation model data are available at <https://earthexplorer.usgs.gov>. The GUB dataset is available at <https://data-starcloudpcl.ac.cn/resource/14>. The GISA

v.2.0 dataset can be obtained from http://irsip.whu.edu.cn/resources/resources_en_v2.php. The dataset of global future urban expansion can be obtained from the National Tibetan Plateau Data Center (<https://doi.org/10.11888/HumanNat.tpdc.272853>). The TerraClimate dataset is available from <https://www.climateologylab.org/terraclimate.html>. The GDP and HDI data were obtained from <https://datadryad.org/stash/dataset/doi:10.5061/dryad.dk1j0>. The WorldPop gridded population density dataset is available at <https://hub.worldpop.org/project/categories?id=18>. The gridded datasets for population and economy under Shared Socioeconomic Pathways are available from the Science Data Bank (<https://doi.org/10.57760/sciencedb.01683>). The nine CMIP6 model outputs can be obtained from the Institute Pierre-Simon Laplace server (<https://esgf-node.ipsl.upmc.fr/search/cmip6-ipsl/>). The administration area data used for mapping were obtained from <https://www.naturelearthdata.com/downloads/50m-cultural-vectors/>.

Code availability

The scripts for performing the analysis in Google Earth Engine (<https://earthengine.google.com/>), drafting the figures in MATLAB R2021b and estimating the projected urban vegetation changes in R v.4.2.2 are available from <https://doi.org/10.5281/zenodo.14630847> (ref. 61). The scripts for performing the main analysis in Google Earth Engine can also be obtained from https://code.earthengine.google.com/?accept_repo=users/171830520nju/Urbanization_global.

References

1. *World City Report 2022: Envisaging the Future of Cities* (UN-Habitat, 2022).
2. *2018 Revision of World Urbanization Prospects* (United Nations, Department of Economic and Social Affairs, 2018).
3. Sun, L., Chen, J., Li, Q. & Huang, D. Dramatic uneven urbanization of large cities throughout the world in recent decades. *Nat. Commun.* **11**, 5366 (2020).
4. Jedwab, R. & Vollrath, D. Urbanization without growth in historical perspective. *Explor. Econ. Hist.* **58**, 1–21 (2015).
5. Grimm, N. B. et al. Global change and the ecology of cities. *Science* **319**, 756–760 (2008).
6. Aronson, M. F. J. et al. A global analysis of the impacts of urbanization on bird and plant diversity reveals key anthropogenic drivers. *Proc. R. Soc. B* **281**, 20133330 (2014).
7. Hao, L. et al. Urbanization alters atmospheric dryness through land evapotranspiration. *npj Clim. Atmos. Sci.* **6**, 149 (2023).
8. Qian, Y. et al. Urbanization impact on regional climate and extreme weather: current understanding, uncertainties, and future research directions. *Adv. Atmos. Sci.* **39**, 819–860 (2022).
9. Gregg, J. W., Jones, C. G. & Dawson, T. E. Urbanization effects on tree growth in the vicinity of New York City. *Nature* **424**, 183–187 (2003).
10. Vitousek, P. M., Mooney, H. A., Lubchenco, J. & Melillo, J. M. Human domination of Earth's ecosystems. *Science* **277**, 494–499 (1997).
11. Zhang, Z., Zhao, W., Liu, Y. & Pereira, P. Impacts of urbanisation on vegetation dynamics in Chinese cities. *Environ. Impact Assess. Rev.* **103**, 10727 (2023).
12. Paschalidis, A., Chakraborty, T., Faticchi, S., Meili, N. & Manoli, G. Urban forests as main regulator of the evaporative cooling effect in cities. *AGU Adv.* **2**, e2020AV000303 (2021).
13. Ziter, C. D., Pedersen, E. J., Kucharik, C. J. & Turner, M. G. Scale-dependent interactions between tree canopy cover and impervious surfaces reduce daytime urban heat during summer. *Proc. Natl Acad. Sci. USA* **116**, 7575–7580 (2019).
14. Du, H. et al. Exacerbated heat stress induced by urban browning in the Global South. *Nat. Cities* <https://doi.org/10.1038/s44284-024-00184-9> (2025).

15. Venter, Z. S., Hassani, A., Stange, E., Schneider, P. & Castell, N. Reassessing the role of urban green space in air pollution control. *Proc. Natl Acad. Sci. USA* **121**, e2306200121 (2024).
16. Veerkamp, C. J. et al. A review of studies assessing ecosystem services provided by urban green and blue infrastructure. *Ecosyst. Serv.* **52**, 101367 (2021).
17. McDonald, R. I. et al. Current inequality and future potential of US urban tree cover for reducing heat-related health impacts. *npj Urban Sustain.* **4**, 18 (2024).
18. Li, L. et al. Competition between biogeochemical drivers and land-cover changes determines urban greening or browning. *Remote Sens. Environ.* **287**, 113481 (2023).
19. Zhang, W., Randall, M., Jensen, M. B., Brandt, M. & Wang, Q. Socio-economic and climatic changes lead to contrasting global urban vegetation trends. *Glob. Environ. Change* **71**, 102385 (2021).
20. Bille, R. A., Jensen, K. E. & Buitenwerf, R. Global patterns in urban green space are strongly linked to human development and population density. *Urban For. Urban Green.* **86**, 127980 (2023).
21. Czekajlo, A. et al. The urban greenness score: a satellite-based metric for multi-decadal characterization of urban land dynamics. *Int. J. Appl. Earth Obs. Geoinf.* **93**, 102210 (2020).
22. Zhao, S., Liu, S. & Zhou, D. Prevalent vegetation growth enhancement in urban environment. *Proc. Natl Acad. Sci. USA* **113**, 6313–6318 (2016).
23. Guan, X., Shen, H., Li, X., Gan, W. & Zhang, L. A long-term and comprehensive assessment of the urbanization-induced impacts on vegetation net primary productivity. *Sci. Total Environ.* **669**, 342–352 (2019).
24. Zhang, L. et al. Direct and indirect impacts of urbanization on vegetation growth across the world's cities. *Sci. Adv.* **8**, eab0095 (2022).
25. Yang, L., Zhao, S. & Liu, S. Urban environments provide new perspectives for forecasting vegetation phenology responses under climate warming. *Glob. Change Biol.* **29**, 4383–4396 (2023).
26. Wang, S. et al. Urban–rural gradients reveal joint control of elevated CO₂ and temperature on extended photosynthetic seasons. *Nat. Ecol. Evol.* **3**, 1076–1085 (2019).
27. Wachsmuth, D. & Angelo, H. Green and gray: new ideologies of nature in urban sustainability policy. *Ann. Am. Assoc. Geogr.* **108**, 1038–1056 (2018).
28. Chang, Y. et al. Effects of climate, socioeconomic development, and greening governance on enhanced greenness under urban densification. *Resour. Conserv. Recycl.* **206**, 107624 (2024).
29. Winbourne, J. B. et al. Tree transpiration and urban temperatures: current understanding, implications, and future research directions. *Bioscience* **70**, 576–588 (2020).
30. Justice, C. O. et al. The Moderate Resolution Imaging Spectroradiometer (MODIS): land remote sensing for global change research. *IEEE Trans. Geosci. Remote Sens.* **36**, 1228–1249 (1998).
31. Huang, X. et al. Toward accurate mapping of 30-m time-series global impervious surface area (GISA). *Int. J. Appl. Earth Obs. Geoinf.* **109**, 102787 (2022).
32. Elith, J., Leathwick, J. R. & Hastie, T. A working guide to boosted regression trees. *J. Anim. Ecol.* **77**, 802–813 (2008).
33. He, W. et al. Global urban fractional changes at a 1 km resolution throughout 2100 under eight scenarios of Shared Socioeconomic Pathways (SSPs) and Representative Concentration Pathways (RCPs). *Earth Syst. Sci. Data* **15**, 3623–3639 (2023).
34. Jiang, T. et al. National and provincial population and economy projection databases under Shared Socioeconomic Pathways (SSP1-5_v2[DS/OL]). V4. *Science Data Bank* <https://doi.org/10.57760/sciencedb.01683> (2022).
35. Chakraborty, T. et al. Large disagreements in estimates of urban land across scales and their implications. *Nat. Commun.* **15**, 9165 (2024).
36. Smith, D. A. Overurbanization reconceptualized: a political economy of the world-system approach. *Urban Aff. Q.* **23**, 270–294 (1987).
37. Wolch, J. R., Byrne, J. P. Urban green space, public health, and environmental justice: the challenge of making cities ‘just green enough’. *Landsc. Urban Plan.* **125**, 234–244 (2014).
38. Pandey, B., Breisford, C. & Seto, K. C. Infrastructure inequality is a characteristic of urbanization. *Proc. Natl Acad. Sci. USA* **119**, 4–11 (2022).
39. Zhou, Y. et al. Satellite mapping of urban built-up heights reveals extreme infrastructure gaps and inequalities in the Global South. *Proc. Natl Acad. Sci. USA* **119**, e2214813119 (2022).
40. Chen, B. et al. Contrasting inequality in human exposure to greenspace between cities of Global North and Global South. *Nat. Commun.* **13**, 4636 (2022).
41. Johnston, R. B. Arsenic and the 2030 agenda for sustainable development. In *Proc. 6th International Congress on Arsenic in the Environment, AS 2016* (eds Bhattacharya, P. et al.) <http://digilibRARY.un.org/record/3923923> (CRC Press, 2016).
42. Shi, Q., Liu, M., Marinoni, A. & Liu, X. UGS-1m: fine-grained urban green space mapping of 31 major cities in China based on the deep learning framework. *Earth Syst. Sci. Data* **15**, 555–577 (2023).
43. Zhang, X. et al. Urban core greening balances browning in urban expansion areas in China during recent decades. *J. Remote Sens.* **4**, 0112 (2024).
44. Chen, Y., Yue, W. & La Rosa, D. Which communities have better accessibility to green space? An investigation into environmental inequality using big data. *Landsc. Urban Plan.* **204**, 103919 (2020).
45. Li, X. et al. Mapping global urban boundaries from the global artificial impervious area (GAIA) data. *Environ. Res. Lett.* **15**, 094044 (2020).
46. Myneni, R., Knyazikhin, Y. & Park, T. MOD15A2H - MODIS/Terra Leaf Area Index/FPAR 8-Day L4 Global 500 m SIN Grid V061 (NASA LP DAAC, 2021).
47. Abatzoglou, J. T., Dobrowski, S. Z., Parks, S. A. & Hegewisch, K. C. TerraClimate, a high-resolution global dataset of monthly climate and climatic water balance from 1958–2015. *Sci. Data* **5**, 170191 (2018).
48. Kummu, M., Taka, M. & Guillaume, J. H. A. Gridded global datasets for Gross Domestic Product and Human Development Index over 1990–2015. *Sci. Data* **5**, 180004 (2018).
49. Sorichetta, A. et al. High-resolution gridded population datasets for Latin America and the Caribbean in 2010, 2015, and 2020. *Sci. Data* **2**, 150045 (2015).
50. Jing, C. et al. Population, urbanization and economic scenarios over the Belt and Road region under the Shared Socioeconomic Pathways. *J. Geogr. Sci.* **30**, 68–84 (2020).
51. Copernicus DEM - Global and European Digital Elevation Model (COP-DEM) (Copernicus DSE, 2020); <https://doi.org/10.5270/ESAC5d3d65>
52. Friedl, M. & Sulla-Menashe, D. MCD12Q1 MODIS/Terra Aqua Land Cover Type Yearly L3 Global 500 m SIN Grid V006 (NASA LP DAAC, 2019).
53. Wu, T. et al. The Beijing Climate Center Climate System Model (BCC-CSM): the main progress from CMIP5 to CMIP6. *Geosci. Model Dev.* **12**, 1573–1600 (2019).
54. Swart, N. C. et al. The Canadian Earth System Model version 5 (CanESM5.0.3). *Geosci. Model Dev.* **12**, 4823–4873 (2019).
55. Wyser, K. et al. On the increased climate sensitivity in the EC-Earth model from CMIP5 to CMIP6. *Geosci. Model Dev.* **13**, 3465–3474 (2020).

56. Dunne, J. P. et al. The GFDL Earth System Model Version 4.1 (GFDL-ESM 4.1): overall coupled model description and simulation characteristics. *J. Adv. Model. Earth Syst.* **12**, e2019MS002015 (2020).
57. Lurton, T. et al. Implementation of the CMIP6 forcing data in the IPSL-CM6A-LR model. *J. Adv. Model. Earth Syst.* **12**, e2019MS001940 (2020).
58. Volodin, E. M. et al. Simulation of the modern climate using the INM-CM48 climate model. *Russ. J. Numer. Anal. Math. Model.* **33**, 367–374 (2018).
59. Mauritsen, T. et al. Developments in the MPI-M Earth System Model version 1.2 (MPI-ESM1.2) and its response to increasing CO₂. *J. Adv. Model. Earth Syst.* **11**, 998–1038 (2019).
60. Zhao, J., Zhao, X., Wu, D., Meili, N. & Fatichi, S. Satellite-based evidence highlights a considerable increase of urban tree cooling benefits from 2000 to 2015. *Glob. Change Biol.* **29**, 3085–3097 (2023).
61. Chen, J. Contrasting effects of urbanization on vegetation between Global South and Global North. Zenodo <https://doi.org/10.5281/zenodo.14630847> (2025).

Acknowledgements

This research was supported by the National Natural Science Foundation of China (42175136, 42130602), and the Jiangsu Collaborative Innovation Center for Climate Change. T.C.'s contribution was supported by the US Department of Energy (DOE), Office of Science, Biological and Environmental Research programme through an Early Career award. Pacific Northwest National Laboratory is operated for DOE by Battelle Memorial Institute under contract DE-AC05-76RL01830. We also thank the dataset providers for sharing the data.

Author contributions

J.C. developed the conceptual framework of this research, performed the analysis and drafted the figures. J.C. and B.Q. drafted the initial version of the manuscript. B.Q. and W.G. provided conceptualization

and supervision, and carried out funding acquisition. T.C., Y.Q., X.M., Y.C., L.L., S.Z., Y.N., X.T. and W.G. contributed to writing the final paper and the interpretation of the results.

Competing interests

The authors declare no competing interests.

Additional information

Extended data is available for this paper at <https://doi.org/10.1038/s41893-025-01520-0>.

Supplementary information The online version contains supplementary material available at <https://doi.org/10.1038/s41893-025-01520-0>.

Correspondence and requests for materials should be addressed to Bo Qiu or Weidong Guo.

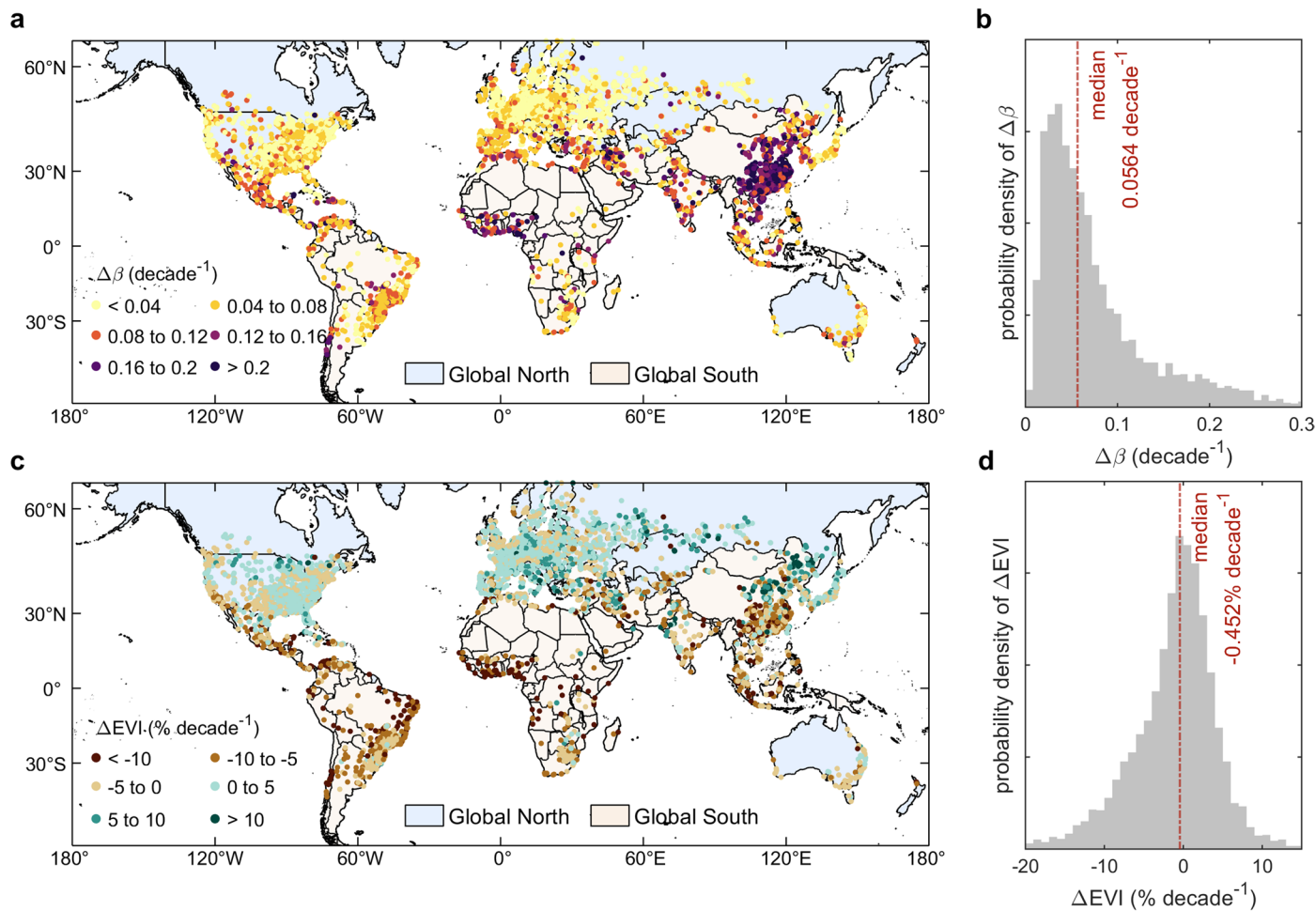
Peer review information *Nature Sustainability* thanks Amanda Cooper and the other, anonymous, reviewer(s) for their contribution to the peer review of this work.

Reprints and permissions information is available at www.nature.com/reprints.

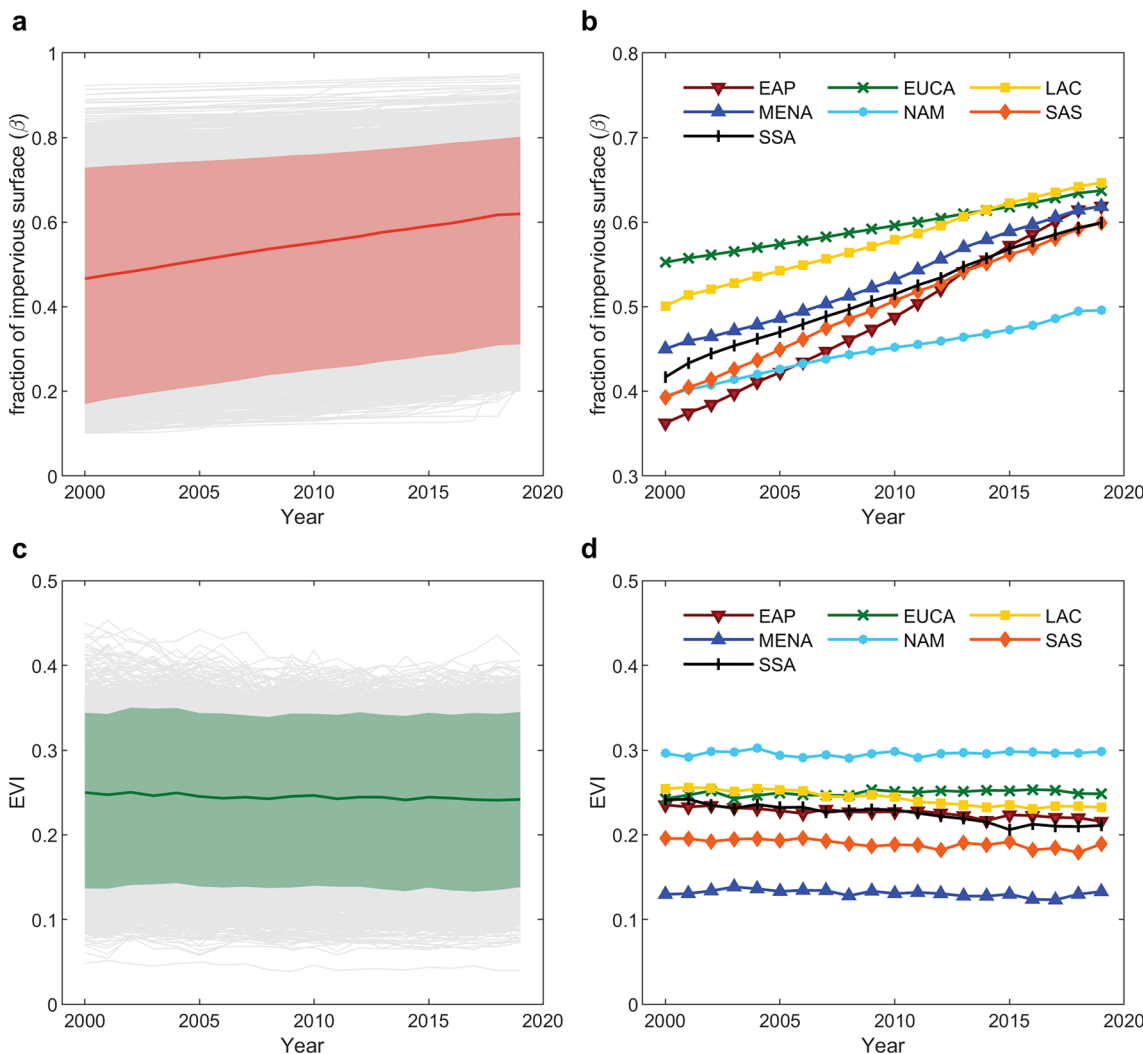
Publisher's note Springer Nature remains neutral with regard to jurisdictional claims in published maps and institutional affiliations.

Springer Nature or its licensor (e.g. a society or other partner) holds exclusive rights to this article under a publishing agreement with the author(s) or other rightsholder(s); author self-archiving of the accepted manuscript version of this article is solely governed by the terms of such publishing agreement and applicable law.

© The Author(s), under exclusive licence to Springer Nature Limited 2025

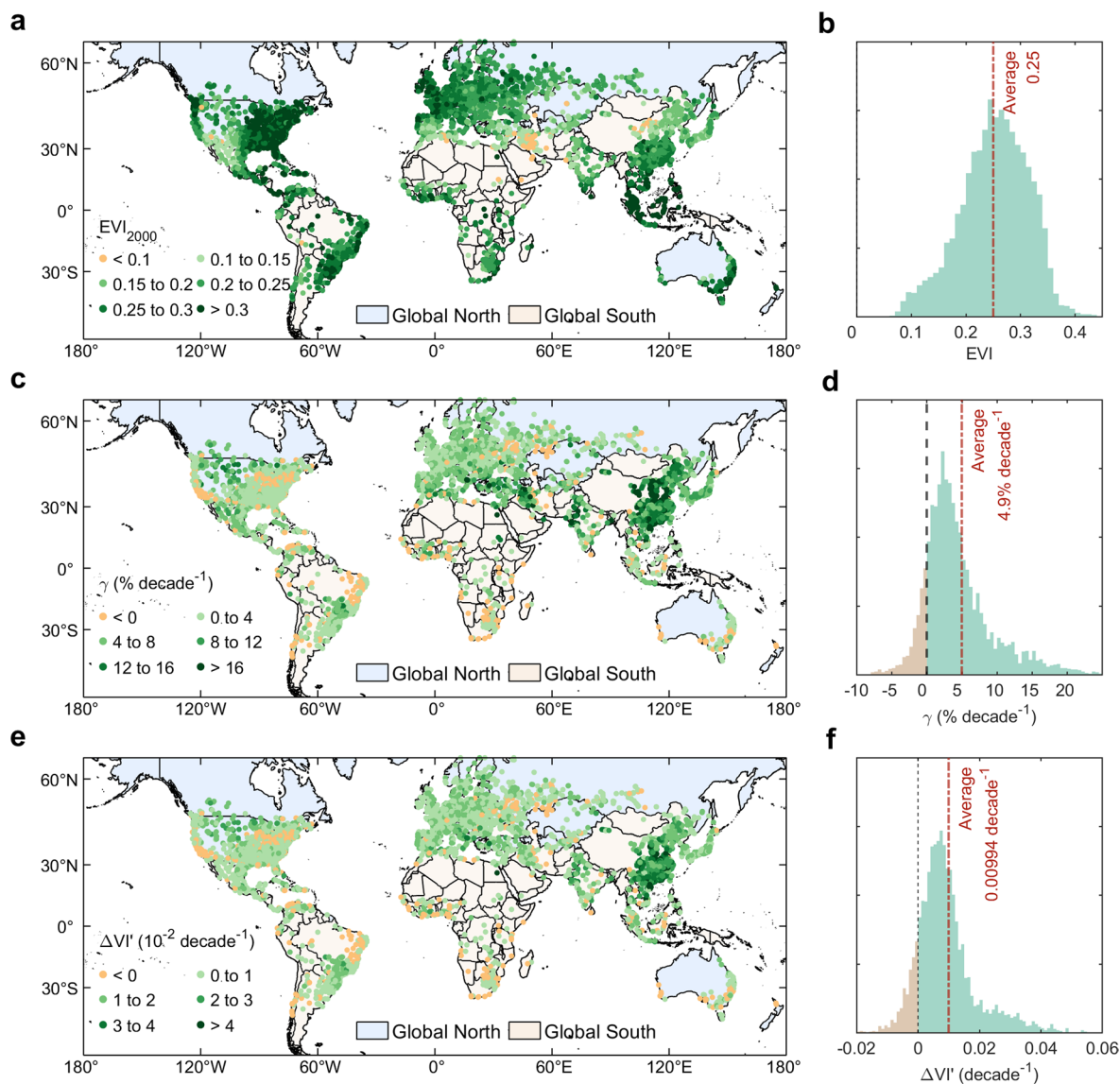


Extended Data Fig. 1 | Changes in the fractions of impervious surfaces area ($\Delta\beta$) and EVI in urban areas during 2000–2019 for global cities. **a, c**, The spatial pattern of $\Delta\beta$ (a) and ΔEVI (c) for global 4718 cities. **b, d**, Histogram of the probability density of cities with different $\Delta\beta$ (b) and ΔEVI (d). The red line represents the medium $\Delta\beta$ and ΔEVI of the cities.



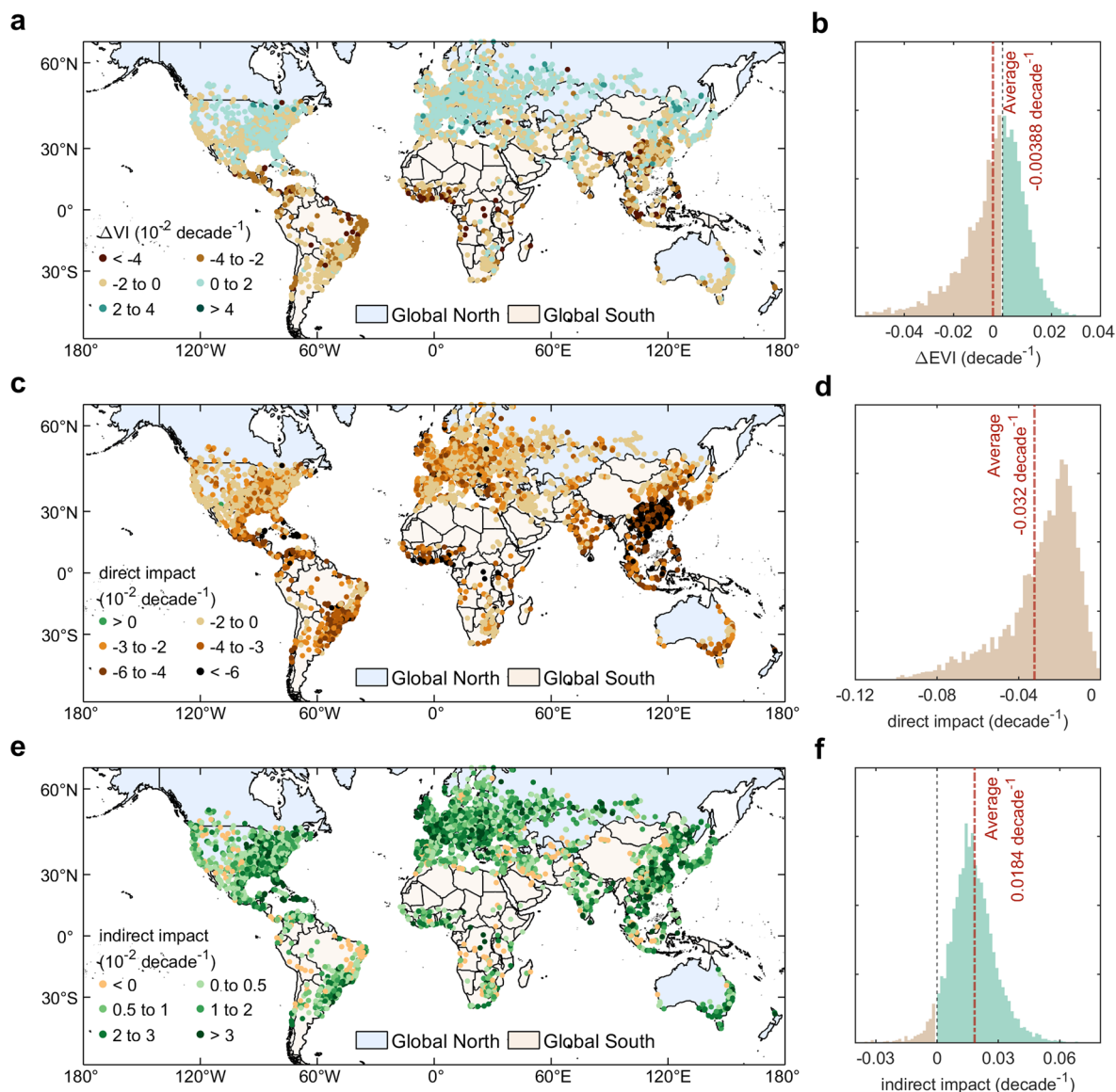
Extended Data Fig. 2 | Temporal trends of the fraction of impervious surfaces (β) and EVI in urban areas for global cities. **a,b**, The average fraction of impervious surfaces (β) for (a) all 4718 cities and (b) seven parts of the world during 2000–2020. **c,d**, Same as **a,b** but for EVI. EAS: East Asia and the Pacific, 963 cities; ECS, Europe and Central Asia, 1512 cities; LCN: Latin America and

Caribbean, 553 cities; MEA: Middle East and North Africa, 142 cities; NAC: North America, 1202 cities; SAS: South Asia, 80 cities; SSF: Sub-Saharan Africa, 266 cities. The shaded ranges in **a** and **c** denote the range of 5–95% β or EVI for global 4718 cities.



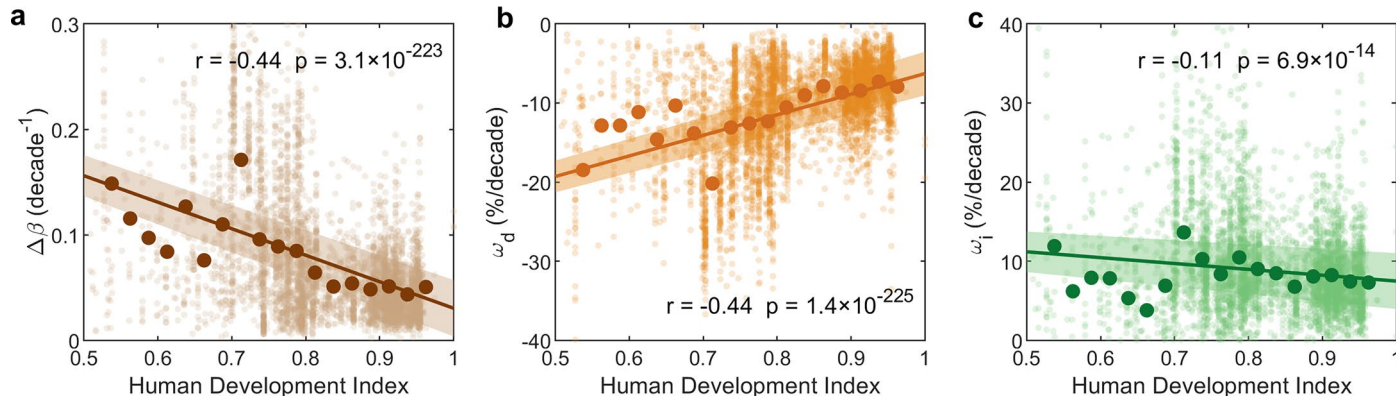
Extended Data Fig. 3 | Effects of macroclimate changes on vegetation growth across cities worldwide. **a**, EVI in 2000 for cities worldwide. **b**, Probability density of cities with different EVIs in 2000. **c**, The extent of vegetation growth enhancement driven by macroclimate change (γ) for global cities during 2000–2019. **d**, Probability density of cities with different γ . **e**, Hypothetical

EVI changes (VI') only driven by macroclimate changes (without considering the increased urbanization) for global cities during 2000–2019. **f**, Probability density of cities with different VI' . The red lines are the average values of each variable of the cities weighted by the urban area.



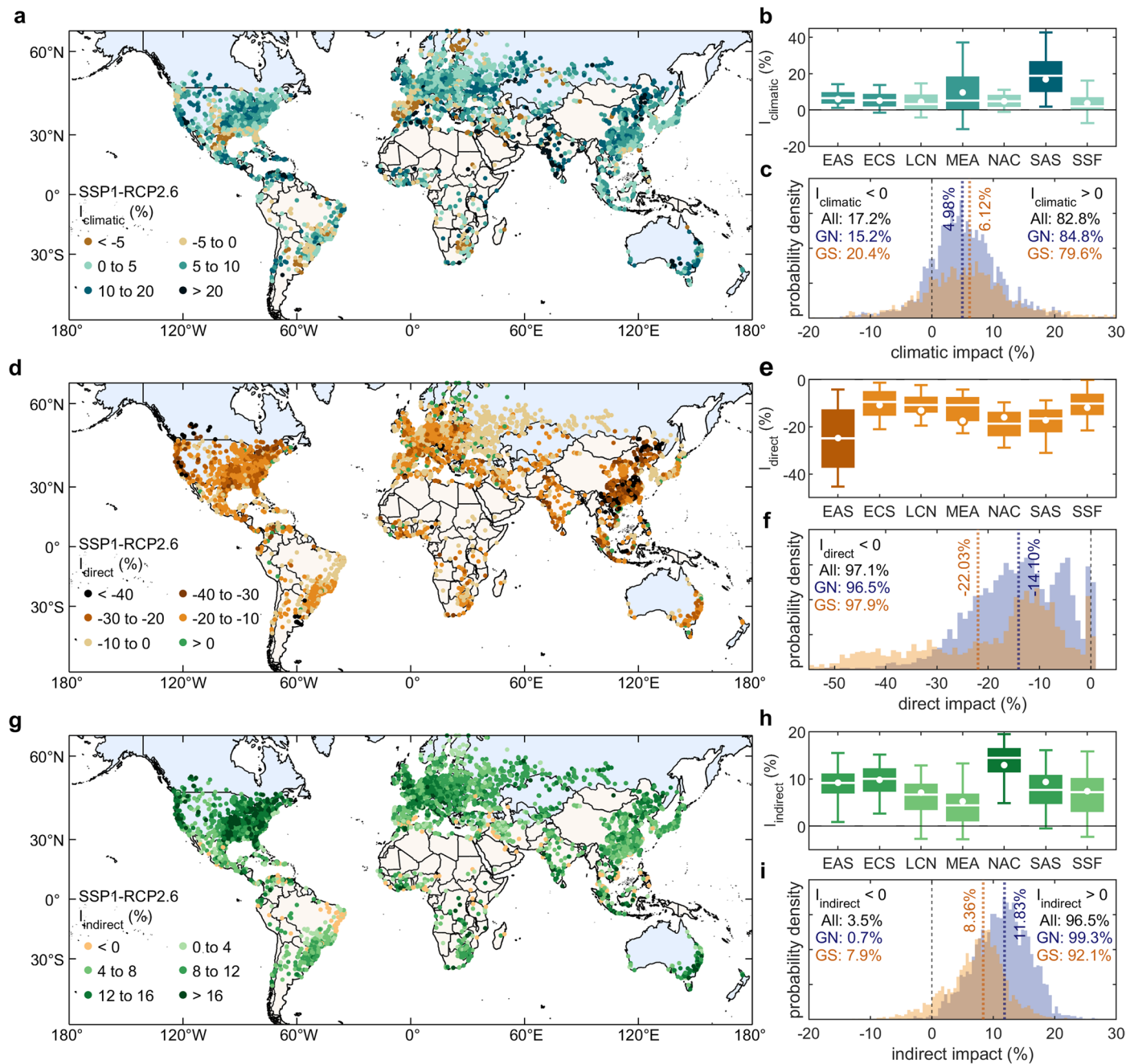
Extended Data Fig. 4 | Direct and indirect impacts of urbanization on vegetation greenness from 2000 to 2019. **a**, Changes of average EVI in urban areas (ΔEVI) from 2000 to 2019 for global cities. **b**, Probability density of cities with different ΔEVI s. **c,e**, Same as **a** but for the EVI changes induced by the

(c) direct and **(e)** indirect impacts of urbanization. **d,f**, Same as **b** but for the direct impact **(d)** and indirect **(f)** impacts on the EVI from 2000 to 2019. The red lines are the average values of EVI and the direct and indirect impacts of cities weighted by urban areas.



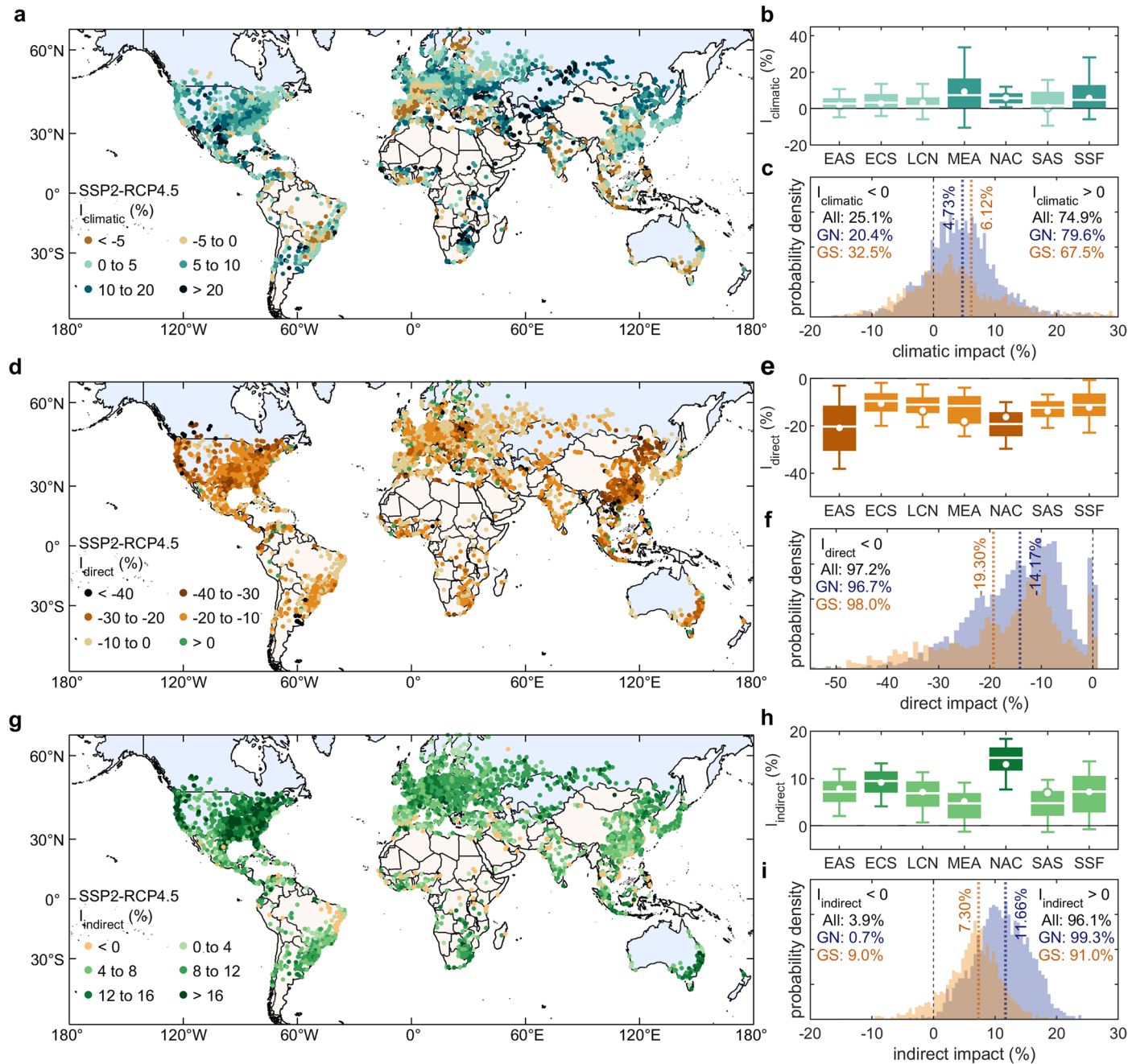
Extended Data Fig. 5 | The effect of socioeconomic development levels on the direct and indirect impacts of urbanization on vegetation greenness. **a**, The relationship between the rate of urban expansion ($\Delta\beta$) and Human Development Index (HDI). The solid lines indicate significant trends, and the shaded areas represent 95% confidence intervals. The small dots denote global 4718 cities and

the big dots denote the average $\Delta\beta$ for cities in each 0.025 HDI bin. Significance was determined by two-side Student's t-test ($P = 3.1 \times 10^{-223}$, $n = 4718$). **b**, Same as **a** but for the direct effects on vegetation (ω_d) ($P = 1.4 \times 10^{-225}$, $n = 4718$). **c**, Same as **a** but for the indirect effects (ω_i) ($P = 6.9 \times 10^{-14}$, $n = 4718$).



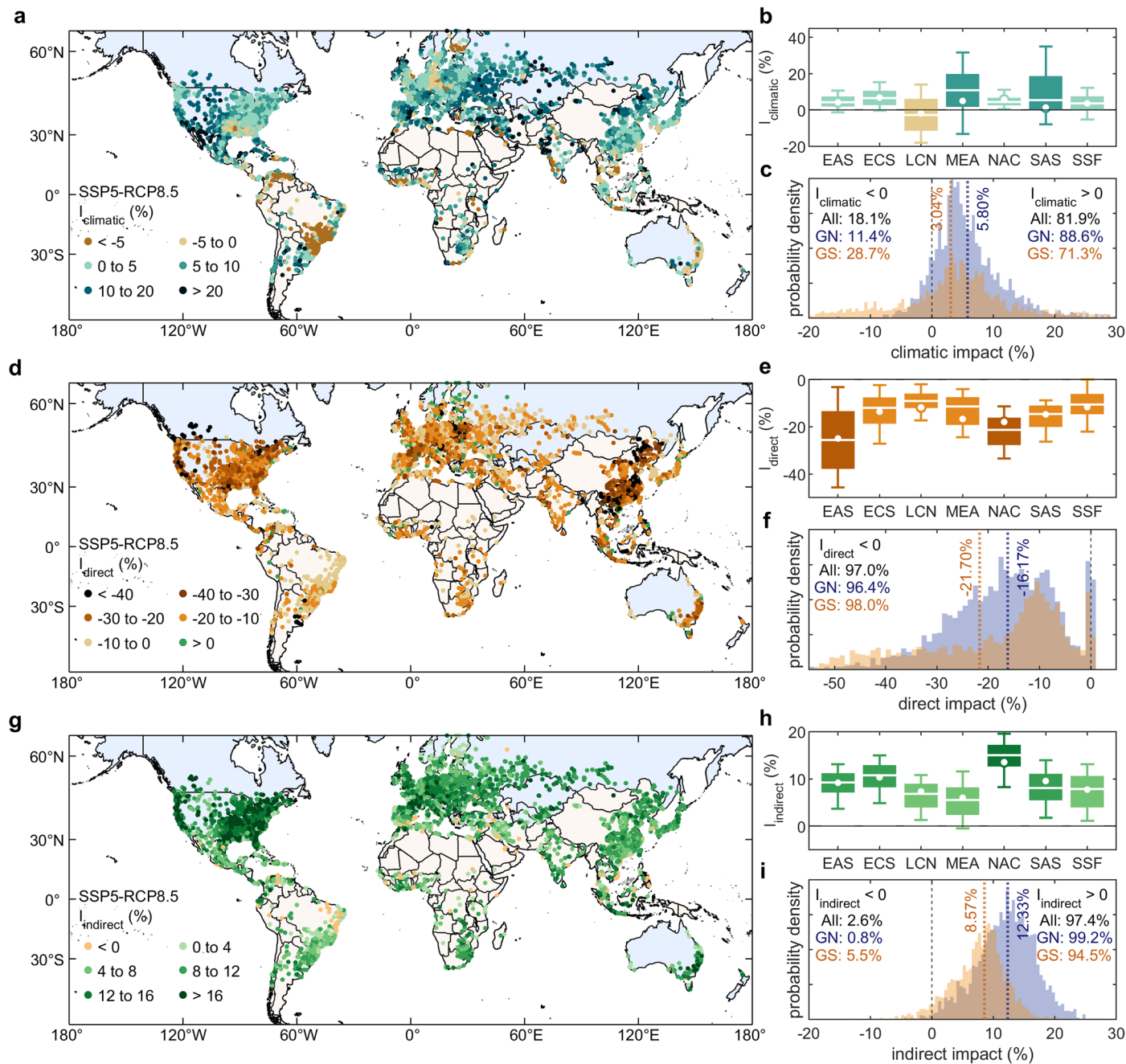
Extended Data Fig. 6 | The projected direct, indirect and climatic impacts on vegetation greenness for global cities under the SSP1-RCP2.6 scenario from 2020 to 2040. **a**, Estimated impacts of macroclimate changes on the EVI by 2040 across global cities under SSP1-RCP2.6 scenario. **b**, Climatic impact on the EVI for cities in different regions across the world. EAS: East Asia and the Pacific, 963 cities; ECS: Europe and Central Asia, 1512 cities; LCN: Latin America and Caribbean, 553 cities; MEA: Middle East and North Africa, 142 cities; NAC: North America, 1202 cities; SAS: South Asia, 80 cities; SSF: Sub-Saharan Africa, 266 cities. The white dots represent the average climatic impact on the EVI

weighted by urban areas for each region. The shaded boxes and vertical lines represent the ranges of 25–75% and 10–90%, respectively. **c**, The probability distributions of climatic impacts for the cities in the Global North and Global South. The dotted lines are the average climatic impacts weighted by urban areas for GN cities and GS cities. The numbers are the proportions of cities with positive or negative climatic impacts. **d–f**, Same as **a–c** but for projected direct impacts of urbanization. **g–i**, Same as **a–c** but for projected indirect impacts of urbanization.



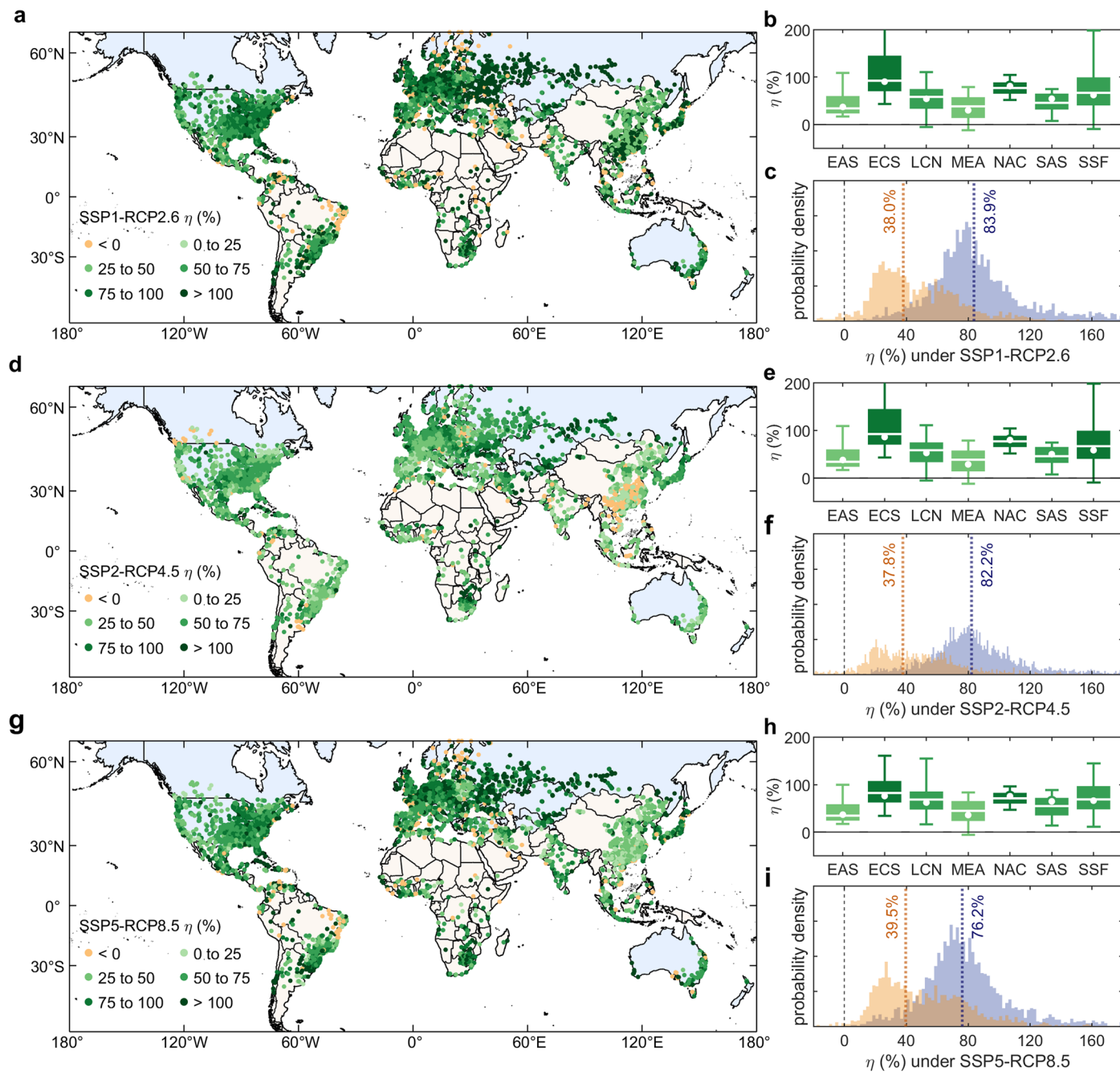
Extended Data Fig. 7 | The projected direct, indirect and climatic impacts on vegetation greenness for global cities under the SSP2-RCP4.5 scenario from 2020 to 2040. **a**, Estimated impacts of macroclimate changes on the EVI by 2040 across global cities under SSP2-RCP4.5 scenario. **b**, Climatic impact on the EVI for cities in different regions across the world. EAS: East Asia and the Pacific, 963 cities; ECS, Europe and Central Asia, 1512 cities; LCN: Latin America and Caribbean, 553 cities; MEA: Middle East and North Africa, 142 cities; NAC: North America, 1202 cities; SAS: South Asia, 80 cities; SSF: Sub-Saharan Africa, 266 cities. The white dots represent the average climatic impact on the EVI

weighted by urban areas for each region. The shaded boxes and vertical lines represent the ranges of 25–75% and 10–90%, respectively. **c**, The probability distributions of climatic impacts for the cities in the Global North and Global South. The dotted lines are the average climatic impacts weighted by urban areas for GN cities and GS cities. The numbers are the proportions of cities with positive or negative climatic impacts. **d–f**, Same as **a–c** but for projected direct impacts of urbanization. **g–i**, Same as **a–c** but for projected indirect impacts of urbanization.



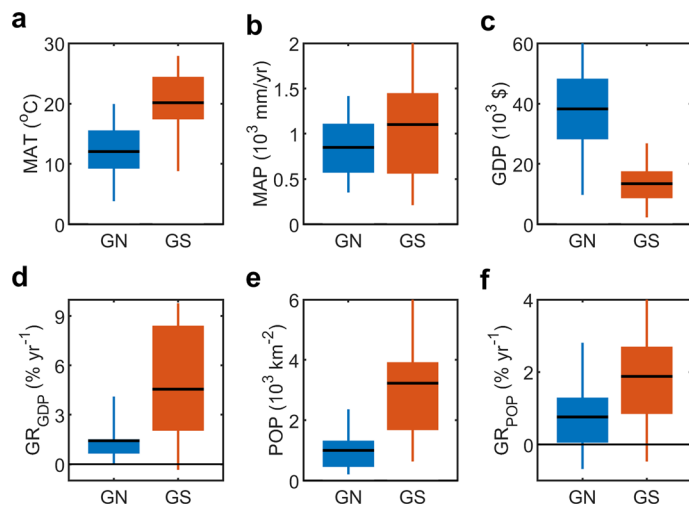
Extended Data Fig. 8 | The projected direct, indirect and climatic impacts on vegetation greenness for global cities under the SSP5-RCP8.5 scenario from 2020 to 2040. **a**, Estimated impacts of macroclimate changes on the EVI by 2040 across global cities under SSP5-RCP8.5 scenario. **b**, Climatic impact on the EVI for cities in different regions across the world. EAS: East Asia and the Pacific, 963 cities; ECS, Europe and Central Asia, 1512 cities; LCN: Latin America and Caribbean, 553 cities; MEA: Middle East and North Africa, 142 cities; NAC: North America, 1202 cities; SAS: South Asia, 80 cities; SSF: Sub-Saharan Africa, 266 cities. The white dots represent the average climatic impact on the EVI

weighted by urban areas for each region. The shaded boxes and vertical lines represent the ranges of 25–75% and 10–90%, respectively. **c**, The probability distributions of climatic impacts for the cities in the Global North and Global South. The dotted lines are the average climatic impacts weighted by urban areas for GN cities and GS cities. The numbers are the proportions of cities with positive or negative climatic impacts. **d–f**, Same as **a–c** but for projected direct impacts of urbanization. **g–i**, Same as **a–c** but for projected indirect impacts of urbanization.



Extended Data Fig. 9 | The projected offsetting coefficients (η) of indirect impacts to direct impacts for global cities under different Shared Socioeconomic Pathways from 2020 to 2040. **a**, Estimated η across global cities under SSP1-RCP2.6 scenario. **b**, The η for cities in different regions across the world. EAS: East Asia and the Pacific, 963 cities; ECS, Europe and Central Asia, 1512 cities; LCN: Latin America and Caribbean, 553 cities; MEA: Middle East and North Africa, 142 cities; NAC: North America, 1202 cities; SAS: South Asia,

80 cities; SSF: Sub-Saharan Africa, 266 cities. The white dots represent the average climatic impact on the EVI weighted by urban areas for each region. The shaded boxes and vertical lines represent the ranges of 25–75% and 10–90%, respectively. **c**, The probability distribution of η for cities in Global North and Global South. The dotted lines are the average η weighted by urban areas for the GN cities and GS cities. **d–f**, Same as **a–c** but for η under the SSP2-RCP4.5 scenario. **g–i**, Same as **a–c** but for η under the SSP5-RCP8.5 scenario.



Extended Data Fig. 10 | Differences in climatic and socioeconomic characteristic between Global North cities and Global South cities. The distributions of (a) mean annual temperature, (b) mean annual precipitation, (c) GDP per capita, (d) compound annual growth rate of GDP per capita, (e) population density, and (f) compound annual growth rate of population

density the cities in the GS ($n = 2888$) and GN ($n = 1830$). The black lines represent the average value of each variable for the GS cities and GN cities. The shaded boxes and the vertical lines represent the ranges of 25–75% and 5–95%, respectively.

Reporting Summary

Nature Portfolio wishes to improve the reproducibility of the work that we publish. This form provides structure for consistency and transparency in reporting. For further information on Nature Portfolio policies, see our [Editorial Policies](#) and the [Editorial Policy Checklist](#).

Statistics

For all statistical analyses, confirm that the following items are present in the figure legend, table legend, main text, or Methods section.

n/a Confirmed

- The exact sample size (n) for each experimental group/condition, given as a discrete number and unit of measurement
- A statement on whether measurements were taken from distinct samples or whether the same sample was measured repeatedly
- The statistical test(s) used AND whether they are one- or two-sided
Only common tests should be described solely by name; describe more complex techniques in the Methods section.
- A description of all covariates tested
- A description of any assumptions or corrections, such as tests of normality and adjustment for multiple comparisons
- A full description of the statistical parameters including central tendency (e.g. means) or other basic estimates (e.g. regression coefficient) AND variation (e.g. standard deviation) or associated estimates of uncertainty (e.g. confidence intervals)
- For null hypothesis testing, the test statistic (e.g. F , t , r) with confidence intervals, effect sizes, degrees of freedom and P value noted
Give P values as exact values whenever suitable.
- For Bayesian analysis, information on the choice of priors and Markov chain Monte Carlo settings
- For hierarchical and complex designs, identification of the appropriate level for tests and full reporting of outcomes
- Estimates of effect sizes (e.g. Cohen's d , Pearson's r), indicating how they were calculated

Our web collection on [statistics for biologists](#) contains articles on many of the points above.

Software and code

Policy information about [availability of computer code](#)

Data collection Most datasets are obtained from Google Earth Engine, and others are downloaded from sources using web browsers.

Data analysis Data processing is carried out in Google Earth Engine (<https://earthengine.google.com/>), MATLAB R2021b, R v4.2.2.

For manuscripts utilizing custom algorithms or software that are central to the research but not yet described in published literature, software must be made available to editors and reviewers. We strongly encourage code deposition in a community repository (e.g. GitHub). See the Nature Portfolio [guidelines for submitting code & software](#) for further information.

Data

Policy information about [availability of data](#)

All manuscripts must include a [data availability statement](#). This statement should provide the following information, where applicable:

- Accession codes, unique identifiers, or web links for publicly available datasets
- A description of any restrictions on data availability
- For clinical datasets or third party data, please ensure that the statement adheres to our [policy](#)

The datasets in this study are publicly available as following or can be obtained from the Google Earth Engine as well. MODIS vegetation greenness data (MOD13A1) and land cover data (MCD13Q1) are available at <https://ladsweb.modaps.eosdis.nasa.gov>. GTOPO30 digital elevation model data are available at <https://eartheexplorer.usgs.gov>. The GUB dataset is available at <https://data-starcloudpcl.ac.cn/resource/14>. The GISA v2.0 dataset can be obtained from http://irsip.whu.edu.cn/resources/resources_en_v2.php. The dataset of global future urban expansion can be obtained from the National Tibetan Plateau Data Center

(<https://doi.org/10.11888/HumanNat.tpdcc.272853>). The TerraClimate dataset is available from <https://www.climatologylab.org/terraclimate.html>. The GDP and HDI data are obtained from <https://datadryad.org/stash/dataset/doi:10.5061/dryad.dk1j0>. The WorldPop gridded population density dataset are available at <https://hub.worldpop.org/project/categories?id=18>. The gridded datasets for population and economy under Shared Socioeconomic Pathways are available from the Science Data Bank (<https://doi.org/10.57760/sciencebd.01683>). The nine CMIP6 model outputs can be obtained from the Institute Pierre-Simon Laplace server (<https://esgf-node.ipsl.upmc.fr/search/cmip6-ipsl/>). The administration areas data used for mapping is obtained from <https://www.naturalearthdata.com/downloads/50m-cultural-vectors/>.

Human research participants

Policy information about [studies involving human research participants and Sex and Gender in Research](#).

Reporting on sex and gender	<input checked="" type="checkbox"/> There were no human participants in the study.
Population characteristics	<input type="checkbox"/> See above
Recruitment	<input type="checkbox"/> See above
Ethics oversight	<input type="checkbox"/> See above

Note that full information on the approval of the study protocol must also be provided in the manuscript.

Field-specific reporting

Please select the one below that is the best fit for your research. If you are not sure, read the appropriate sections before making your selection.

Life sciences Behavioural & social sciences Ecological, evolutionary & environmental sciences

For a reference copy of the document with all sections, see nature.com/documents/nr-reporting-summary-flat.pdf

Ecological, evolutionary & environmental sciences study design

All studies must disclose on these points even when the disclosure is negative.

Study description	This study provide a framework to quantify the direct and indirect impacts of urbanization on the temporal dynamics of vegetation greenness, considering the effects of large-scale climate change on vegetation growth.
Research sample	The 4718 cities are analyzed in this study, including both large and small cities across the world.
Sampling strategy	The cities with an urban area greater than 10 km ² are analyzed, which covers most of the world's cities.
Data collection	Most datasets are obtained from Google Earth Engine, and others are downloaded from sources using web browsers.
Timing and spatial scale	The historical period is 2000-2019, and the future period is 2020-2040 in this study. The data is aggregated to annual averages on a city scale for analysis.
Data exclusions	Only the pixels that satisfied the two hypotheses of the adjacent substitution method are used, and the cities with enough valid pixels are analyzed.
Reproducibility	The results are reproducible if the methods described in the article are followed.
Randomization	The data are not from a random sampling, and randomization is not involved.
Blinding	Blinding methods are not involved in this study.

Did the study involve field work? Yes No

Reporting for specific materials, systems and methods

We require information from authors about some types of materials, experimental systems and methods used in many studies. Here, indicate whether each material, system or method listed is relevant to your study. If you are not sure if a list item applies to your research, read the appropriate section before selecting a response.

Materials & experimental systems

n/a	Involved in the study
<input checked="" type="checkbox"/>	Antibodies
<input checked="" type="checkbox"/>	Eukaryotic cell lines
<input checked="" type="checkbox"/>	Palaeontology and archaeology
<input checked="" type="checkbox"/>	Animals and other organisms
<input checked="" type="checkbox"/>	Clinical data
<input checked="" type="checkbox"/>	Dual use research of concern

Methods

n/a	Involved in the study
<input checked="" type="checkbox"/>	ChIP-seq
<input checked="" type="checkbox"/>	Flow cytometry
<input checked="" type="checkbox"/>	MRI-based neuroimaging

Terms and Conditions

Springer Nature journal content, brought to you courtesy of Springer Nature Customer Service Center GmbH (“Springer Nature”).

Springer Nature supports a reasonable amount of sharing of research papers by authors, subscribers and authorised users (“Users”), for small-scale personal, non-commercial use provided that all copyright, trade and service marks and other proprietary notices are maintained. By accessing, sharing, receiving or otherwise using the Springer Nature journal content you agree to these terms of use (“Terms”). For these purposes, Springer Nature considers academic use (by researchers and students) to be non-commercial.

These Terms are supplementary and will apply in addition to any applicable website terms and conditions, a relevant site licence or a personal subscription. These Terms will prevail over any conflict or ambiguity with regards to the relevant terms, a site licence or a personal subscription (to the extent of the conflict or ambiguity only). For Creative Commons-licensed articles, the terms of the Creative Commons license used will apply.

We collect and use personal data to provide access to the Springer Nature journal content. We may also use these personal data internally within ResearchGate and Springer Nature and as agreed share it, in an anonymised way, for purposes of tracking, analysis and reporting. We will not otherwise disclose your personal data outside the ResearchGate or the Springer Nature group of companies unless we have your permission as detailed in the Privacy Policy.

While Users may use the Springer Nature journal content for small scale, personal non-commercial use, it is important to note that Users may not:

1. use such content for the purpose of providing other users with access on a regular or large scale basis or as a means to circumvent access control;
2. use such content where to do so would be considered a criminal or statutory offence in any jurisdiction, or gives rise to civil liability, or is otherwise unlawful;
3. falsely or misleadingly imply or suggest endorsement, approval , sponsorship, or association unless explicitly agreed to by Springer Nature in writing;
4. use bots or other automated methods to access the content or redirect messages
5. override any security feature or exclusionary protocol; or
6. share the content in order to create substitute for Springer Nature products or services or a systematic database of Springer Nature journal content.

In line with the restriction against commercial use, Springer Nature does not permit the creation of a product or service that creates revenue, royalties, rent or income from our content or its inclusion as part of a paid for service or for other commercial gain. Springer Nature journal content cannot be used for inter-library loans and librarians may not upload Springer Nature journal content on a large scale into their, or any other, institutional repository.

These terms of use are reviewed regularly and may be amended at any time. Springer Nature is not obligated to publish any information or content on this website and may remove it or features or functionality at our sole discretion, at any time with or without notice. Springer Nature may revoke this licence to you at any time and remove access to any copies of the Springer Nature journal content which have been saved.

To the fullest extent permitted by law, Springer Nature makes no warranties, representations or guarantees to Users, either express or implied with respect to the Springer nature journal content and all parties disclaim and waive any implied warranties or warranties imposed by law, including merchantability or fitness for any particular purpose.

Please note that these rights do not automatically extend to content, data or other material published by Springer Nature that may be licensed from third parties.

If you would like to use or distribute our Springer Nature journal content to a wider audience or on a regular basis or in any other manner not expressly permitted by these Terms, please contact Springer Nature at

onlineservice@springernature.com